Rui Wang

# Combined Effects of The Electromagnetic Suspension and Frequency-Velocity Dependent Reaction Force of The Guideway on The Hyperloop Instability

TU Delft

# Combined Effects of The Electromagnetic Suspension and Frequency-Velocity Dependent Reaction Force of The Guideway on The Hyperloop Instability

## One-Dimensional Euler-Bernoulli Beam Model Case

By

Rui Wang

in partial fulfilment of the requirements for the degree of

**Master of Science**
in Civil Engineering

at the Delft University of Technology,
to be defended publicly on Friday December 23, 2022 at 10:45 AM.

Student number: 5240484
Thesis committee:
Dr. ir. K. Van Dalen, TU Delft, supervising chair
Prof. dr. ir. A. V. Metrikine, TU Delft, supervisor
Ir. A. Faragau TU Delft, weekly supervisor



TU Delft

# Preface

Time flies, my master's career at TUD comes to an end. As a civil engineering student, I never knew this discipline was so fascinating before, especially when I touched dynamics, I was deeply attracted by its charm. Of course, it is not easy to follow the courses at the beginning, sometimes it can even be said to be painful. Fortunately, TUD also taught me how to endure loneliness and persist on the things you love.

Karel van Dalen is my initiation teacher in Dynamics and I'm deeply impressed by his passion and profession in this field. That's why I had no hesitation to find him for the master thesis. Firstly, I'm very grateful to him to trust me and provide me this opportunity to take part in this project. Then, I want to appreciate the other members (Andrei Metrikine and Andrei Faragau) of my committee with my highest respect for all the help and support, especially my daily supervisors Andrei Faragau who has been such patient from the beginning to the end and taught me how to think as a scientist rather than an engineer. I also want to thank professor Andrei Metrikine for his wisdom perspectives in each progress meeting which always inspire me to jump out of the box.

Finally, I'd like to share the happiness of graduation with my family and friends for their consistent companionship and unconditional trust. I can't make it without them in the first hardest year due to Covid-19. Thanks, and I love you all.

*Rui Wang*
*Delft, December 2022*

# Abstract

The stability analysis of electromagnetic suspension system applied to Hyperloop in simplified two degrees of freedom system has been studied deeply where the track-beam is regarded as a point mass and the effects of velocity and beam are neglected. However, there is little reference on the study of the interaction between electromagnetic suspension system and wave effects.

The main aim of this thesis is to investigate the dynamic behavior of the EMS vehicle-beam coupled system using the one-dimensional model, and illustrate the combined effects of the EMS and guideway on the vehicle instability at different horizontal velocity by comparing with the results of EMS system in simplified model and mechanical system in one-dimensional model.

Along these lines, the tube is modelled as an infinite long Euler-Bernoulli beam resting on a homogenous viscoelastic foundation and the vehicle is modelled as a point mass. The response of the system is obtained both numerically and analytically. The values of control gains are determined based on the equivalent simplified two degrees of freedom EMS system. A representative mechanical system is designed to show the anomalous Doppler waves effects. It is found that for inappropriate values of control gains which will cause instability of vehicle at static state, the one-dimensional guideway has positive effects which can stabilize the vehicle at certain range of subcritical velocity, whereas for appropriate values of control gains the EMS system can counteract the wave-induced instability and keeps the vehicle stable at even supercritical velocity. Finally, a method to linearize the system is presented which allows eigenvalue analysis.

# List of Contents

# 1. Introduction

## 1.1. Background

The world enters an era of information globalization, people can learn about the world through a variety of media, such as TV, mobile phones, computers and so on. Certainly, people are not satisfied with discovering the world through the aforementioned media, they also need to explore this beautiful world themselves. Therefore, people's demand for a faster, more efficient, more environmentally friendly and cheaper mode of transportation is increasing day by day. Along these lines, the market share for high-speed transportation is increasing rapidly and it is predicted that by 2050 that around half of the total traffic in the world will be high-speed transportation [1].

Nowadays, people can choose to travel by air or by high-speed rail. In the last decade or so, high-speed rail has developed very rapidly and has become popular all over the world, and there are many countries in the world that use high-speed railroads in large numbers, such as China, Japan and the whole of Europe. In the short and medium distance transportation (200-1000 km), high-speed railroad has many obvious advantages over aviation: first, the whole journey time is short (save time to and from the airport, waiting time for plane); second, the delivery capacity is large; third, the impact on climate change is small and the on-time rate is high. Nevertheless, for journeys of more than 1,000 kilometers, airplanes can show their superiority in speed and convenience. In addition, airplanes can leap over almost all kinds of natural obstacles and reach places that are difficult to reach by rail or road. At the same time, their shortcomings are also obvious. For high-speed rail, the fares are usually expensive and it has great impact on residents along the line, such as noise and vibration pollution. For aviation, it has a very high carbon footprint. In 2018, global aviation (i.e., commercial, freight and military aviation) represented a 2.5% of the total CO2 emissions worldwide and, with respect to non-CO2 climate impacts, it accounts for 3.5% of the global warming [2]. Thus, attempts have been made to find an alternative of transportation that retains their advantages while avoiding the disadvantages.

Hyperloop is a form of transportation based on the theory of "vacuum tube transport", which is also known as vactrain. This concept can be traced back to the 18$^{th}$ century, in 1799, when a man named George Medhurst from London conceived of and patented an atmospheric railway that could convey people or cargo through pressurized or evacuated tubes. At that time, the design relied on steam power propulsion. Then in 1904, the name ‘vactrain’ was firstly invented by Robert H. Goddard and he imagined that in the future people could travel in a mag lev train that shot at high speed through an airless tunnel [3]. On the basis of this concept, the idea was future improved and developed in 20$^{th}$ century.

Time comes to 2013, a term named by ‘Hyperloop’ is proposed as an open-sourced technological concept and any other company or research institutes in the world has been encouraged to take the ideas and further develop them [4]. Hyperloop designs employ three essential components: tubes, pods, and terminals. The tube is a large sealed, low-pressure system (usually a long tunnel). The pod is a coach pressurized at atmospheric pressure that runs substantially free of air resistance or friction inside this tube using aerodynamic or magnetic propulsion [5]. The terminal handles pod arrivals and departures. The speed of hyperloop may be even higher than 1000km/h [6] which is even faster than airplane but with less emission as electricity is the energy source. It is hoped in the future that hyperloop can replace high-speed rail and flights with the advantages of ultra-high speed, high safety, low energy consumption, low noise, low pollution, etc.

## 1.2. Problem Statement

With the increase of speed, especially for supercritical velocity (explained in section 2.5.1), the problem of wave-induced instability can occur depending on the nature (mass, stiffness, etc.) of the system and increase the risk of the transportation significantly. What's more, the electromagnetic suspension itself is dynamically unstable if there is no control [7]. Besides, the model of tube used in this thesis is one-dimensional beam with infinite degrees of freedom and the system of equations of motion consists of both non-linear force and partial differential equation (beam), it cannot be solved analytically as there is no reference to deal with such system by far. Hence, this thesis firstly tries to find a numerical method to solve this set of equations, then it seeks proper control to stabilize the system with certain horizontal velocity of vehicle and shows the effects of the electromagnetic suspension system on vehicle instability in hyperloop at different velocities. Last but not least, to reveal the nature of this kind of system, attempts have been made to linearize this kind of system.

The sketch (*Figure 1. 1*) below illustrates a longitudinal cut of the vehicle and the track infrastructure of the Hardt Hyperloop design. It is helpful for us to better understand the problem addressed.

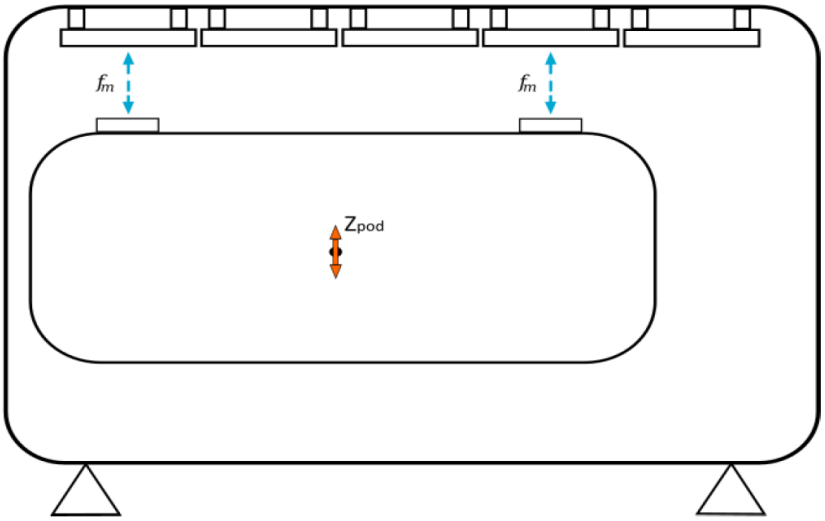


*Figure 1. 1 Longitudinal cut of Hyperloop design [8]*

It should also be noted that the design and implementation of electromagnetic suspension systems in Hyperloop contain transdisciplinary concepts such as electromagnetism, mechanical engineering, structural dynamics, etc. Here we only focus on structural dynamic part.

## 1.3. Research Objectives

Almost all available literatures about the stability of EMS consider only the first-order bending mode of beam by which the tube is simplified to a single degree of freedom system, e.g., the study of EMS applied to Hyperloop technologies based on "2.5 degrees of freedom" system is elaborated in [8]. Thus, the first objective in this thesis is:

1. Find a numerical method to simulate the behavior of EMS in "infinite degrees of freedom" system.

    a) Define the set of equation of motion (EOM) in which the tube is regarded as 1-dimensional (1-D) system. Here the tube is modeled as an infinitely long Euler-Bernoulli beam resting on a foundation with distributed spring and dash-pot.

b) Design and validate the numerical methodology to solve the EOM

Once the solution to the non-linear partial differential equation (PDE) system is obtained, one can then predict the response of the system under appropriate closed-loop error-based control (proportional-(P), derivative-(D), PD) and investigate the effects of EMS on vehicle instability under different horizontal velocity.

2. Perform dynamic analysis and stability study of the system at different horizontal velocities of vehicle.

   a) Choose the stiffness of control system to present the representative characteristics of the system in 1-D model

   b) Design a linear mechanical system for comparison

   c) Determine the relationship between velocity and other parameters of interest, i.e., stability, initial perturbations, mass, and control gains.

Unfortunately, one still cannot obtain any information about the nature (eigenvalues, etc.) on the stability of the system when numerical part is finished. Thus, semi-analytical analysis is required after linearization of the system.

3. Linearize the system around the steady-state position and compare the outcome with non-linear system as verification

## 1.4. Report Outline

This report is composed of 4 main parts: a literature review, a chapter introducing the analytical model and the derivation of the equation of motions, a chapter presenting how to solve the non-linear PDE system numerically and its underlying basic assumptions, a chapter presenting an attempt to solve the non-linear PDE system analytically by linearization and the main troubles stuck in the road. The synopsis of each chapter is shown below:

Chapter 2 serves to introduce the reader to all the fundamental engineering concepts they will face in the following research of this thesis, and present the current state as well as the major achievements on the field of electromagnetic suspension technologies. Besides, it also illustrates the control scheme for the stabilization and explains the instability phenomenon in the system composed of moving objects and one-dimensional guide.

Chapter 3 presents the analytical model of the problem addressed in this report and all the presumptions of modelling used to derive of the equations of motion.

Chapter 4 elaborate the idea of the numerical method and its underlying assumptions, after which the dynamic analysis and stability study is performed to illustrate the deficiencies of the simplified model [8] and how the representative mechanical/EMS system will affect the vehicle instability in one-dimensional model.

Chapter 5 presents and corroborates the linearization of the EMS system. What’s more, the effects of EMS system on the accuracy of the linear approximations are illustrated.

Chapter 6 summarizes all the findings obtained from this project and proposes some recommendations for future research on this subject.

# 2. Literature Review and Basic Theoretical Foundation

In this chapter, a review of the relevant literature was conducted in order to address the three main issues raised in the introduction section. To make it easier for the reader to understand the theoretical knowledge framework of the whole thesis, it can be briefly described here in the following 4 areas:

1. The concept of stability and an introduction to the associated conception, such as the flow, fixed point, phase portrait, and bifurcation, etc. What's more, it is also important to note the difference between linear and non-linear systems in terms of stability.

2. The development of electromagnetic levitation technology, an introduction to its applications and the main achievements in this field. Clear the relevant theoretical background knowledge to be used later in this thesis.

3. The basic concepts of the process control.

4. Based on the theoretical model in Chapter 3, this thesis focuses on the system of forces or objects moving with uniform velocity along an infinitely long beam, and therefore here presents a review of the stability issues of this kind of system.

As the first three points are described in detail in Ref. [8], the author will not repeat them the same way but briefly describe them here.

## 2.1.Stability

To understand stability, one can start from instability. The concept of instability can be seen everywhere in life, e.g., buckling of column, a ball on the top of a hill, an inverted pendulum, etc. All the aforementioned objects share a characteristic that when they deviate from the equilibrium point by even a small disturbance, the whole system collapses. However, for a stable system, or more precisely, for an attracting equilibrium point [9], when you give a small perturbation, this perturbation will decay with time and finally go to zero. This will be explained in mathematical language later in this chapter.

There are two main types of dynamical systems: differential equations and iterated maps [9]. Here we only focus on differential equations, and the evolution of the system is continuously time-dependent.

### *2.1.1. Flow and linearization*

The one-dimensional flow can be represented by a dynamic system described as follows

$$\dot{x} = f(x) \tag{2.1}$$

where $x(t)$ is a real-valued function of time t and $f(x)$ is a smooth real-valued function of $x$, $\dot{x}$ stands for the first derivative with respect to time. If $f$ does not depend explicitly on $t$, this is called an autonomous system. Otherwise $f$ would depend explicitly on $t$, the system becomes non-autonomous as the one derived for this project (see in chapter 3).

Then, one could draw the graph of a random $f(x)$ (*Figure 2. 1*)and use it to sketch the vector field on the real line represented by the x-axis. One can imagine there is a fluid flowing along the real line with a local velocity $f(x)$. This imaginary fluid is called the phase fluid and the real line is the phase space. It can be easily told that if $f(x) \succ 0$, $x$ will grow or in other words, the flow is towards the right and vice versa. Now if an imaginary particle called phase point is placed at $x_0$ and one can then observe how it is carried along by this flow. As time goes on, the phase point moves along the x-axis according to some function $x(t)$. This function is called trajectory and it represents the solution of the differential equation starting from the initial condition $x_0$. The representation of one or more trajectories of the system is called a phase portrait (*Figure 2. 1*) [9].

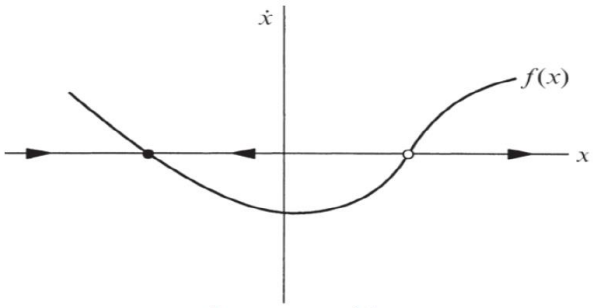


*Figure 2. 1 Phase portrait of the system [9]*

The fixed points $x^*$, defined by $f(x^*) = 0$, regulate how the phase portrait appears. In the illustration shown in *Figure 2. 1*, the solid black dot is called stable fixed point, since the flow is toward it in both sides, and the hollow point is called unstable fixed point, since flow is repelled from it [9]. In fact, fixed points are categorized in great depth [9], only these two are presented here as explannations.

Fixed points are equilibrium solutions (also known as steady, constant, or rest solutions) in the context of the initial differential equation, since if $x = x^*$ initially, then $x(t) = x^*$ for all time. An equilibrium is defined to be stable if all sufficiently small disturbances away from it damp out in time, therefore stable equilibria are represented geometrically by stable fixed points. On the other hand, unstable equilibria are those in which disturbances increase with time and are represented by unstable fixed points [9].

Keep in mind that the concept of stable equilibrium is built on minor disturbances, and for some huge disruptions the system may fail to decay. In such a case, the fixed point in question is defined to be locally stable, but not globally stable. If $x^*$ attracts all trajectories in the phase plane, it then could be called globally stable [9].

However, only graphical approaches have been addressed up to this point for figuring out the stability of fixed points in a qualitative manner. It is necessary to solve an eigenvalue problem for a quantitative evaluation. Unfortunately, non-linear dynamic systems do not have eigenvalues. The system must therefore be linearized around the fixed point as a preliminary step. Here, a straightforward example will be used to explain the steps of linearization, for more complicated cases such as two-dimensional flow, please refer to the book [9].

Let $x^*$ be a fixed point and let $\eta(t) = x(t) - x^*$ which stands for a small perturbation away from $x^*$. To determine if the perturbation grows or decays, a first-order differential equation for $\eta$ needs to be derived [9].

$$\dot{\eta} = \frac{d}{dt}(x - x^*) = \dot{x} = f(x) = f(x^* + \eta) \tag{2.2}$$

Afterwards, one could apply Taylor's expansion to eq. 2.2.

$$f(x^* + \eta) = f(x^*) + \eta f'(x^*) + O(\eta^2) \tag{2.3}$$

Where $O(\eta^2)$ denotes quadratically small terms in $\eta$. Note that $f(x^*) = 0$ since $x^*$ is a fixed point. Then eq. 2.3 could be simplified as

$$\dot{\eta} = \eta f'(x^*) + O(\eta^2) \tag{2.4}$$

Now, assume $f'(x^*) \neq 0$, the $O(\eta^2)$ terms are quite small compared to it as $\eta$ is a small perturbation that can be neglected (note that it is not always safe to neglect the quadratic terms [9], a case-by-case basis is needed). Then one could rewrite the linearized approximation about $x^*$ as [9]

$$\dot{\eta} \approx \eta f'(x^*) \tag{2.5}$$

This shows that the perturbation $\eta$ grows exponentially if $f'(x^*) \succ 0$ and decays if $f'(x^*) \prec 0$. If $f'(x^*) = 0$, the $O(\eta^2)$ terms are no longer negligible and a non-linear analysis is needed to determine stability [9]. Now the new feature is that one finds a way to gauge how stable or unstable a fixed point is. This is determined by the magnitude of $f'(x^*)$. This magnitude plays an important role of an exponential growth or decay rate. Moreover, its reciprocal $1/f'(x^*)$ is a characteristic time scale, it could determine the time required for $x(t)$ to vary significantly in the neighborhood of $x^*$ [9].

Besides one need to make sure the initial value problem consisting of eq. 2.1 and initial condition $x(0) = x_0$ has only one solution, or the stability will be uncertain. Fortunately, there exist a theorem that proves the existence and uniqueness of the solution. This theorem says that if $f(x)$ is smooth enough ( $f(x)$ and $f'(x)$ are continuous on an open interval R of the x-axis), the solutions exist and are unique. Even so, there is no guarantee that solutions exist forever, due to the existence of blow-up phenomena, etc. [9].

### *2.1.2. Limit cycle*

A limit cycle is an isolated closed trajectory and exists only in non-linear systems, i.e., the neighboring trajectories are not closed, but they spiral either towards or away from the limit cycle (*Figure 2. 2*). If all neighboring trajectories approach the limit cycle, the limit cycle is stable or attracting. Otherwise, the limit cycle is unstable, or in some cases, half-stable [9].

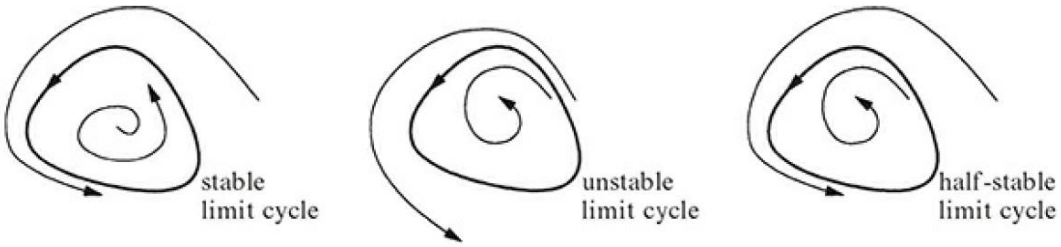


*Figure 2. 2 Limit cycle classification [9]*

Stable limit cycles are very important scientifically, since they model systems that exhibit self-sustained oscillations. In other words, these systems oscillate even in the absence of external periodic forcing. For this kind of system, there is a standard oscillation of some preferred period, waveform, and amplitude. If the system is perturbed slightly, it always returns to the standard cycle [9].

Limit cycles can never occur in linear systems. Of course, a linear system can have closed orbits, but they won't be isolated; if $\mathbf{x}(t)$ is a periodic solution, then so is $c\mathbf{x}(t)$ for any constant $c \neq 0$. Hence $\mathbf{x}(t)$ is surrounded by a one-parameter family of closed orbits (*Figure 2. 3*). As a result, the amplitude of a linear oscillation is totally determined by its initial conditions; any small perturbation in the amplitude will last forever. Limit cycle oscillations, on the other hand, depend on the structure of the system [9].

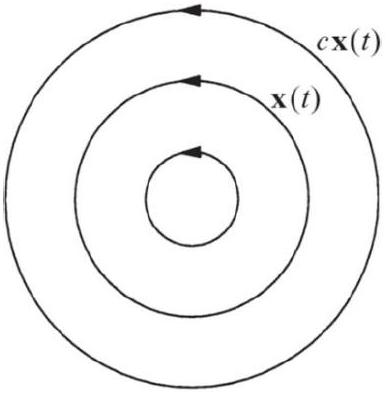


*Figure 2. 3 Parameter family of closed orbits*

### *2.1.3. Bifurcations*

An interesting aspect is that the qualitative structure of the flow described in section 2.1.1 can change as parameters are varied. In particular, fixed point can be created or destroyed, or their stability can change. These qualitative changes in dynamics are called bifurcations and the parameter values at which they occur are called bifurcation points. Bifurcations are important scientifically since they provide models of transitions from stability to instability and vice versa as some control parameter is varied [9].

The most basic bifurcation type is the saddle-node bifurcation, and the involved basic mechanism is that fixed points are created and destroyed. As one parameter is varied, two fixed points move toward each other, collide, and mutually annihilate. The prototypical example of a saddle-node bifurcation is given by the following first-order system

$$\dot{x} = r + x^2 \tag{2.6}$$

Where $r$ is a parameter and may be positive, negative or zero. If $r$ is negative, there are two fixed points, one of which is stable and the other one is unstable (*Figure 2. 4*.a). As $r$ approaches zero from negative, the parabola moves up and the two fixed points move towards each other. When $r = 0$, a half-stable fixed point forms out of the two fixed points at $x^* = 0$ (*Figure 2. 4*.b). This particular fixed point is extremely fragile, as it vanishes once $r \succ 0$ and afterwards, there are no longer fixed points (*Figure 2. 4*.c). In this case, bifurcation occurs at $r = 0$ [9].

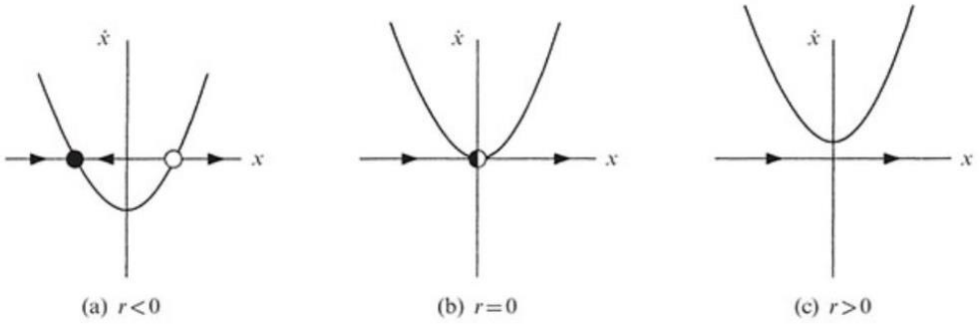


*Figure 2. 4 Saddle-node bifurcation example*

This example is the so-called normal form of the saddle-node bifurcation and in fact, there are certain many representative one-dimensional flow bifurcations like the transcritical bifurcation and the supercritical pitchfork bifurcation [9].

For one-dimensional cases mentioned above, the bifurcation occurs when one of the eigenvalues is zero, such bifurcations are called zero-eigenvalue bifurcations. Here, however, for the two-dimensional flow, a fundamentally new kind of bifurcation is introduced which provides a way for a fixed point to lose stability without colliding with any other fixed points and it's named by Hopf bifurcation which is observed in this thesis. This happens when two complex conjugate eigenvalues simultaneously cross the imaginary axis into the right half-plane. There are two types of Hopf bifurcation: subcritical and supercritical [9].

Suppose we have a physical system that settles down to equilibrium through exponentially damped oscillations (*Figure 2. 5*.a). Now suppose that the decay rate depends on a control parameter $\mu$. If the decay becomes slower and slower and finally changes to growth at a critical value $\mu_c$, the equilibrium state will lose stability. In many cases the resulting motion is a small-amplitude, sinusoidal, limit cycle oscillation about the former steady state (*Figure 2. 5*.b). Then we say that the system has undergone a supercritical Hopf bifurcation [9].

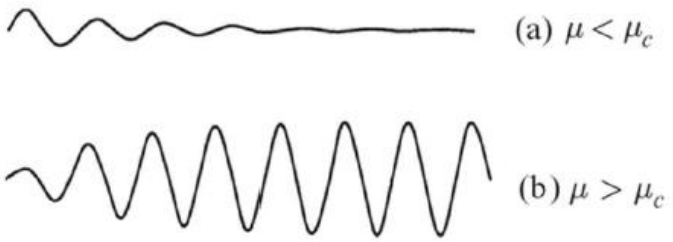


*Figure 2. 5 Equilibrium decay and supercritical bifurcation growth depending on the control parameter [9]*

The subcritical Hopf bifurcation is always much more dramatic, and potentially dangerous in engineering applications. After the bifurcation, the trajectories must jump to a distant attractor, which may be a fixed point, another limit cycle, infinity or, in three and higher dimensions, a chaotic attractor (*Figure 2. 6*) [9].

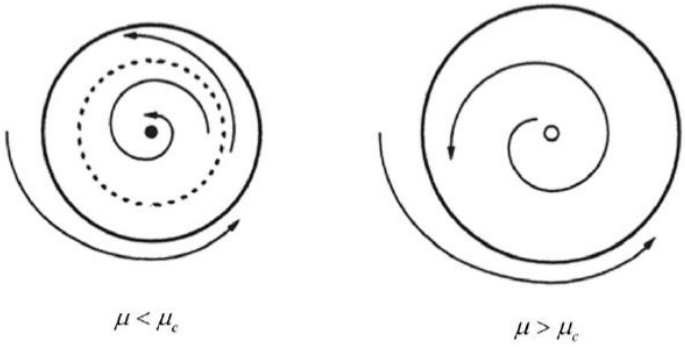


*Figure 2. 6 Phase portraits before and after subcritical Hopf bifurcation happens [9]*

## 2.2.Magnetic levitation techniques

In order to improve the railway's traffic efficiency, the engineers identified the friction at the contact interface between the wheels and the rail as a significant source of energy loss. As a result, over the last century, several engineers have focused on the research of levitating rail infrastructure design, which eliminates friction and allows vehicles to reach higher speeds while also extending the infrastructure's lifetime. In this vein, two major levitation technology designs have been developed: electromagnetic suspension (EMS) and electrodynamic suspension (EDS). Of both the latter has also been divided into two different concepts, one of which uses superconducting electromagnets and the other uses an array of permanent magnets. The last is better known as Inductrack. Each of these levitation techniques is schematically represented in the figure (*Figure 2. 7*) below [8].

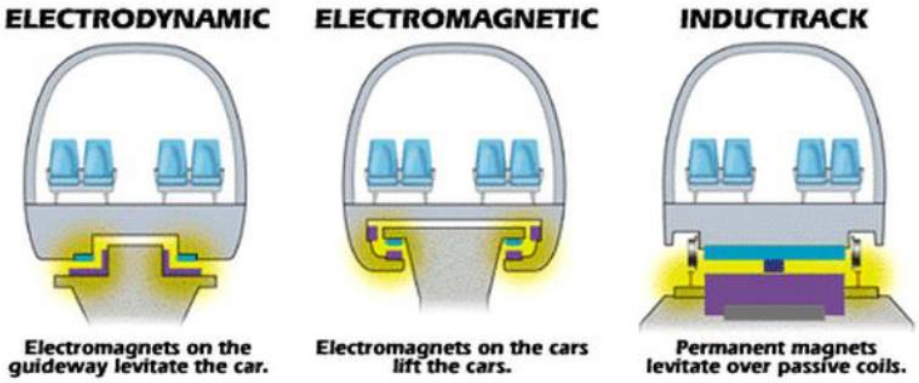


*Figure 2. 7 Representation of the different magnetic levitation systems [10]*

As this project focuses on the application of EMS system on Hyperloop technology, here only describe the principles, pros and cons, major achievements of EMS.

### *2.2.1. Electromagnetic suspension (EMS)*

The EMS system employs the enticing magnetic force of electromagnets installed in the vehicle's support frame (e.g., boogie) to draw the vehicle to a magnetically conductive track and keep it at a predetermined distance from the rails. The electromagnets actively monitor the air gap and keep the train at a constant distance from the track using feedback control systems [11].

Little literature is available on the application of EMS system on Hyperloop. Fortunately, more research has been dedicated to the use of EMS in Maglev trains, which can be extrapolated to our design. For Maglev

trains applications the EMS system can lift a train using attractive forces by the magnets beneath a guide-rail [12]. The electromagnetic field is generated by the onboard suspension electromagnet (or permanent magnet plus excitation control coils) and causes the mutual attraction with the track. This is depicted in the figure below (*Figure 2. 8*) where the vehicle is suspended on a rail. The suspension gap between the electromagnet and the electromagnetic rail is approximately 8-10 mm [13].

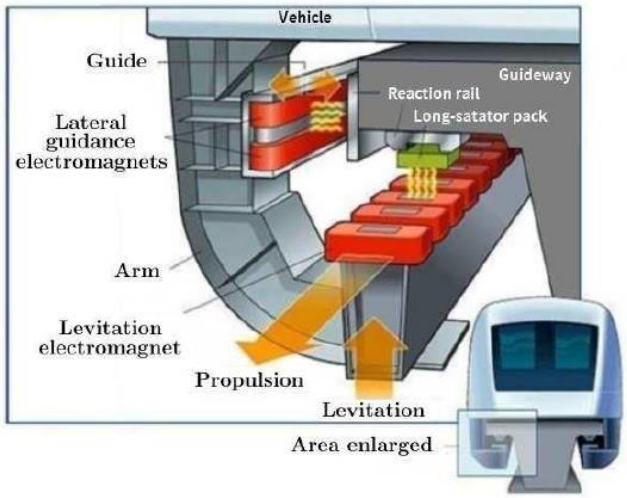


*Figure 2. 8 EMS system used in the Transrapid [10]*

Only one Hyperloop design project, the Hardt Hyperloop, has used this levitation system. Nonetheless, when it comes to Hardt Hyperloop Design, this mechanism's layout changes slightly. In this case, the rail is mounted on the hyperloop tube's ceiling and consists of a magnetically conductive track, and the hybrid permanent magnets are attached to boogie frames that move beneath the rail, as shown in the figure below (*Figure 2. 9*) [8].

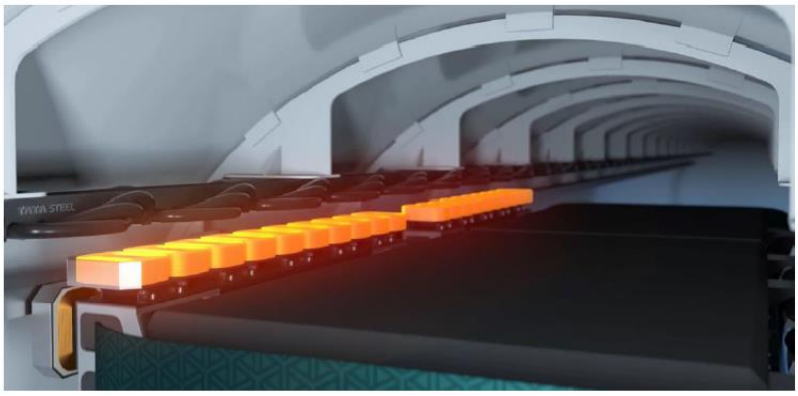

*Figure 2. 9 Initial EMS system in Hardt Hyperloop [14]*

The main advantage of EMS systems is that they can work at all speeds and avoid the disadvantage of EDS that they only work at a minimum speed of about 30 km/h, which can eliminate the requirement for a separate low-speed suspension system and can simplify the track layout as a result [13]. Its application in recently developed Maglev trains has proven that it is a commercially available technology, which can reach a very high speed of up to 500 km/h [11].

In contrast, the main disadvantage of the EMS technology is the dynamically unstable nature of electromagnetic attraction. Samuel Earnshaw showed that it is not possible to place a collection of bodies, subject only to electrostatic forces, in such a way that they remain in a stable equilibrium configuration [7]. This

theorem applies to magnetic forces as well. In fact, it is true for any force that varies with the inverse square of the distance, or any combination of such forces [15]. Thus, a constant monitoring of the levitation air gap is required to control and correct the error by computer systems integrated either on the rail or the vehicle [11].

### *2.2.2. Major achievements*

Numerous studies have been conducted on the stability of EMS Maglev trains traveling through flexible guideways [16-22]. While there are minor variations in the magnet form and the vehicle-infrastructure fitting and interaction, they all generally provide the same design principles for the EMS levitation system. The most variances come from the type of control system used or the guideway modeling.

The most common modelling of the flexible guideway is by simplifying the track beam to a single-span simply supported Euler-Bernoulli beam [16-22]. In these cases, a modal analysis is firstly conducted for the model of the beam in the system, then it is found that the vibration frequency corresponding to the maximum displacement of track beam caused by running of maglev train is distributed within a range, and the first-order frequency of the track beam has the greatest impact [21]. Thus, in most of the papers, only the track beam's first-order bending mode is considered [16-22].

Junxiong Hu et al. analyzed the mechanical characteristics of the system composed of a single electromagnet and elastic track beam, then established a five-dimensional dynamics model of single electromagnet-track beam coupled system under classical PD control strategy. In this paper, based on the Hurwitz algebraic criterion and the high-dimensional Hopf bifurcation theory, the stability of the coupled system is analyzed, proving the existence of a subcritical Hopf bifurcation which is governed by the value $K_p$ [19].

What's more, J. Mas Soldevilla also confirmed the existence of a subcritical Hopf bifurcation for a critical proportional gain parameter $K_p$. It's also noted the implementation of an on/off switch on the electromagnetic force can avoid unrealistic negative electrical current and increase the range of initial conditions under which the system can be stabilized [8].

Nevertheless, the two degrees of freedom system is only a simplification and is not fully correct. Considering the actual system is continuous, the track-beam can be modelled in a more accurate way by regarding as an infinite continuous beam. This will be explained in detail in Chapter 3.

## 2.3.Kirchhoff's law of voltage and current

This thesis presents a model in which the force term is concerned with current, thus it's important to know the basis of electromagnetics especially the relationship between voltage and electric current.

In electromagnetism and electronics, a conductor's inductance is the property by which a change in the current that flows through it causes a voltage or electromotive force in both the conductor itself (i.e., self-inductance) and any nearby conductors (i.e., mutual inductance). A changing electric current through a circuit that contains inductance induces a proportional voltage that opposes the change in current. The relationship among the parameters for a coil with inductance $L$ is defined as [23]

$$V = IR + L\frac{dI}{dt} \tag{2.7}$$

Where $L = \frac{N^2 \mu A}{l}$, other parameters will be explained in detail in Chapter 3.

Now it is important to introduce the concept of Kirchhoff's law of voltage and current which state that "the total voltage around a loop is equal to the sum of all the voltage drops within the same loop" and "the total current or charge entering a junction or node is equal to the charge leaving the node, cause the charge has no other place to go except to leave as no charge is lost within the node", respectively. This will allow us to relate the magnetic and electric variables all in one equation later such that the full behavior of the electromagnet will be captured through the expression below [8]

$$V = IR + L\frac{dI}{dt} - K\frac{d\delta}{dt} \tag{2.8}$$

Where $\delta$ stands for the levitation air gap. Eq. 2.8 establishes the system's total voltage in the way by taking the input from the ohmic term and subtracting the losses brought on by the variations in electrical current flow and the levitation air gap [8].

## 2.4.Control strategies

Process controls are necessary for designing safe and productive plants (here means the vehicle-beam EMS system). Process controls come in many forms, but the PID controller is the most basic and frequently the most efficient. This kind of controller attempts to correct the error between a measured process variable and desired setpoint by calculating the difference and then taking remedial measures to modify the process as necessary. A PID controller controls a process through three parameters: Proportional (P), Integral (I), and Derivative (D). These parameters can be weighted, or tuned, to adjust their effect on the process [24].

This thesis chooses a fundamental approach to design a controller, shaping it as a closed-loop feedback control. The following (*Figure 2. 10*) is a description of a general closed-loop feedback control's primary structure.

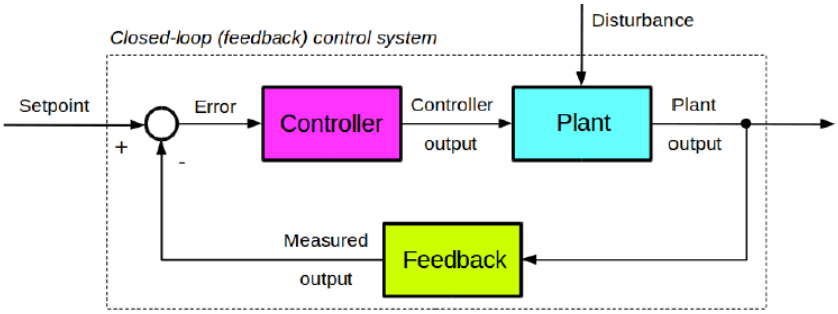


*Figure 2. 10 Closed-loop feedback control [25]*

Where one has to define the reference setpoint $r(t)$ (here initial air gap $r(t) = \delta_0$), the error $e(t)$ which activates the controller defined as the difference between the measured value (air gap $\delta$) and the reference setpoint, the controller transfer function $G_c(t)$ which depends on the control type and controller coefficients ($K_d$, $K_p$), the controller output which is the input of the system $u(t)$ (here the voltage $U$), the plant transfer function $G_p(t)$ which depends on the way of modelling (here non-linear PDE system), the plant output $y(t)$

(here air gap $\delta$), and in some cases, the sensor transfer function $h(t)$. *Figure 2. 11* below presents the symbolic notation for each component outlined in this paragraph.

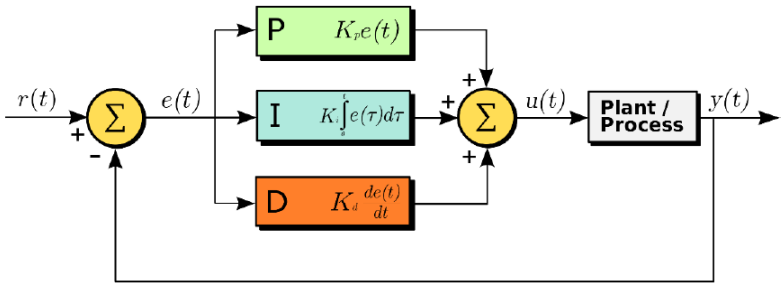


*Figure 2. 11 PID controller closed-loop feedback scheme [26]*

PID-control correlates the controller's output to the error, integral of the error, and derivative of the error. Hence, the PID control function in time domain is defined as

$$u_{PID}(t) = K_p e(t) + K_i \int_0^t e(\tau)d\tau + K_d \frac{de(t)}{dt} \tag{2.9}$$

Where $K_p$ is the proportional gain, $K_i$ is the integral gain, $K_d$ is the derivative gain, $e(t)$ is the error of the system, $u_{PID}(t)$ is the output of controller and $t$ is time. The stability of the system is directly impacted by the controller's coefficients. For certain values of such coefficients un unstable system can be stabilized.

## 2.5.Moving force / object in one-dimensional systems

As this thesis considers the track-beam as an infinitely long Euler-Bernoulli beam resting on a Winkler foundation, it would be good to understand how the associated mechanical systems behave as the main difference of this project and others lies in the non-linear electromagnetic force. The resonance of moving force or instability phenomenon of moving mass in one-dimensional systems has been extensively studied through different models, here briefly elaborate in 2 main directions: 1. Moving force system; 2. Moving mass system.

It can be concluded that for moving force situation, no instability is observed but only the resonance will happen at critical velocity $v_{crit}$. While for cases of interaction with moving mass, at velocities smaller than $v_{crit}$ the vibrations are always stable and at velocities larger than $v_{crit}$ they can be unstable or stable depending on the elastic-inertia properties (mass of the moving object and contact stiffness between the two) of the system.

### *2.5.1. Moving force system*

A.R.M Wolfert described the wave effects in one-dimensional systems interacting with moving loads in great depth [27]. Now imagine a system (*Figure 2. 12*) composed of a force $P$ moving with constant velocity $v$ along an infinitely long Euler-Bernoulli beam which is rest on Winkler foundation. One can write the governing equation of motion (EOM) as follow

$$w'''' + 4\gamma^2 \ddot{w} + 4\beta^4 w = -\frac{P}{EI}\delta(x - vt) \tag{2.10}$$

Where $\gamma = \sqrt{\frac{\rho}{4EI}}$ and $\beta = \sqrt[4]{\frac{k}{4EI}}$. $\rho$ and $EI$ are the mass per unit length and the bending stiffness of the beam, $k$ is the stiffness of the foundation per unit length. For conciseness, the time derivative is replaced by an over dot and the space derivative by a prime. These notations apply to the rest of this thesis**.** In addition, the variables of the functions $x$ and $t$ are left out from the equations.

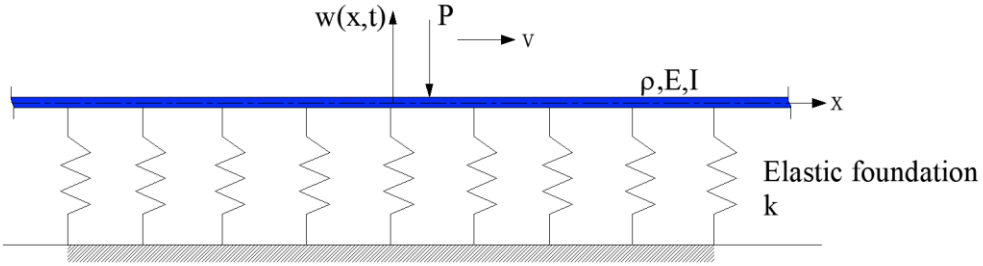


*Figure 2. 12 Moving force system*

This system is solved in [27], one can find that

1. When velocity $v \prec v_{crit}$, in which $v_{crit} = \frac{\beta}{\gamma}$ stands for critical velocity, the steady-state displacement of the beam is depicted as below. The field is called the eigenfield, which moves stationary with the load.

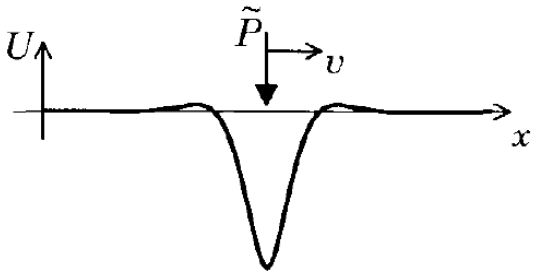


*Figure 2. 13 Steady-state solution of a constant load moving with $v \prec v_{crit}$ [27]*

2. When velocity $v \succ v_{crit}$, the solution is plotted for an arbitrary time moment. The field depicted in *Figure 2. 14* is called Vavilov-Cherenkov (VC) field. A property of this field is that it is asymmetrical with respect to the loading point.

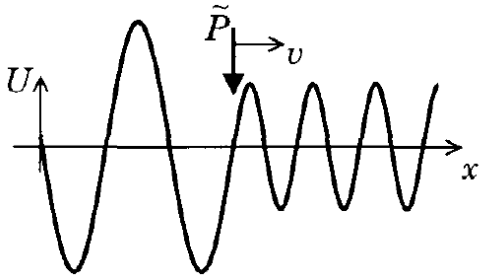


*Figure 2. 14 Steady-state solution of a constant load moving with $v \succ v_{crit}$ [27]*

3. When velocity $v = v_{crit}$, the steady-state solution does not exist and the displacements becomes infinite, in other words, resonance happens.

### 2.5.2. Moving Mass System

A.V. Metrikine has investigated the uniform motion of a mass along an axially compressed Euler-Bernoulli beam on a viscoelastic foundation [28]. The model is depicted in *Figure 2. 15*, and it is assumed that the mass and the beam are in continuous contact and a vertical constant force acts on the moving mass.

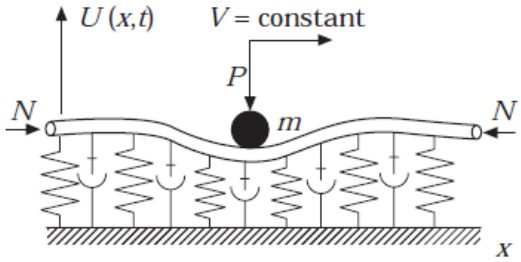


*Figure 2. 15 The uniform motion of a mass (subjected to a constant vertical force) along a beam [28]*

The EOM for the model can be written as

$$\rho\ddot{U} + EIU'''' + NU'' + \mu\dot{U} + \chi U = -(m\ddot{U}^0 + P)\delta(x - Vt) \tag{2.11}$$

Where $U(x,t)$ and $U^0(t)$ are the vertical deflections of the beam and the mass, respectively. $N$ is the compressional force, $\mu$ and $\chi$ are the viscosity and stiffness of the foundation per unit length, $m$, $V$, and $P$ are the mass, velocity and vertical force of the body, $\delta(\cdots)$ is the Dirac delta function.

The main focus of this paper is on the relationship between the instability phenomenon and compressional axial stresses in the beam. *Figure 2. 16* shows the dependency of critical mass $M^*$ (above which the instability happens) versus the velocity.

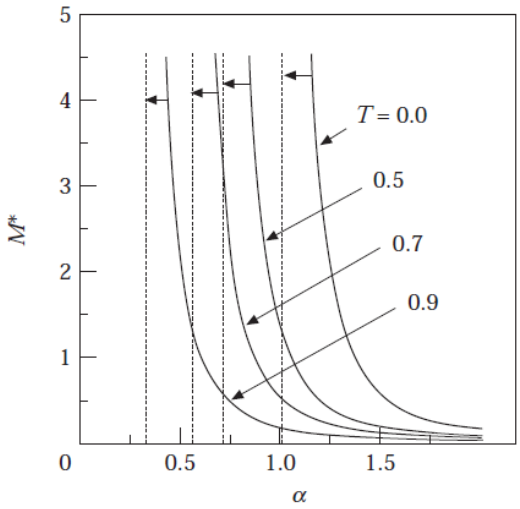


*Figure 2. 16 M* versus $\alpha$ for different compressional forces [28]*

Where $\alpha = \dfrac{v}{v_{crit}}$ stands for the ratio of velocity and critical velocity. The domain located above a curve is associated with unstable vibrations of the beam. One can conclude from the figure (*Figure 2. 16*) that [28]

1. If the beam is not axially compressed, the instability can take place only for $\alpha \succ 1$.

2. The larger the mass, the smaller the velocity that can cause instability.

3. The instability starts at smaller velocities (for a fixed value of mass) when the compressional force increases.

What's more, the correlation of instability of beam and viscosity of foundation is also investigated here (*Figure 2. 17*). The domain located above a line is the instability domain.

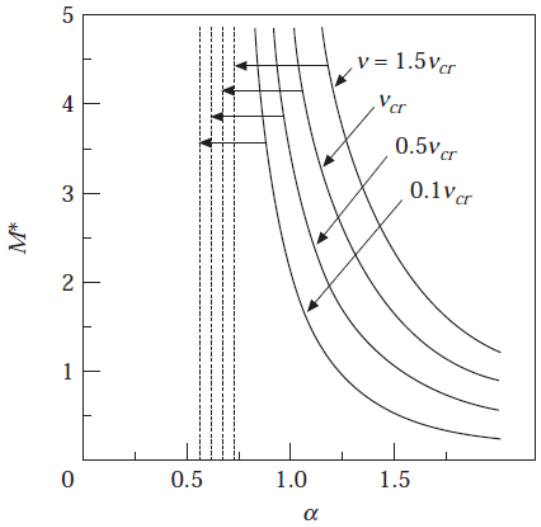


*Figure 2. 17 The dependency M*( $\alpha$ ) for different viscosities of the foundation (T=0.7) [28]*

It should be noted that the instability still occurs for overcritical viscosities, although the instability starts at larger velocities (for a fixed mass) as the viscosity increases. The reason is that the resonance vibration due to the moving load can be effectively damped but the instability resulted from interaction of mass and beam is caused by anomalous Doppler waves [28].

# 3. Modelling of The EMS Levitation System

The model of the EMS levitation established in this chapter is used as the foundation for all analytical study cases presented in this thesis. To be noted, the main purpose of this thesis is to qualitatively elaborate the effects of EMS system in the stability of vehicle-beam coupled system. Hence, the parameters of the model are not representative for Hardt Hyperloop, but are chosen from the known model of rail-structure [29].

In this case, the following assumptions have been adopted:

1. Considering the tube's length is much larger than its diameter and neglecting the shear stiffness of itself, the tube is modelled as an Euler-Bernoulli beam.

2. The beam is supported by a uniformly distributed spring-dash-pot foundation.

3. The length of the vehicle is relatively small compared to that of tube. Thus, the vehicle is considered as a point mass.

To this end, the overview of the model is illustrated below (*Figure 3. 1*).

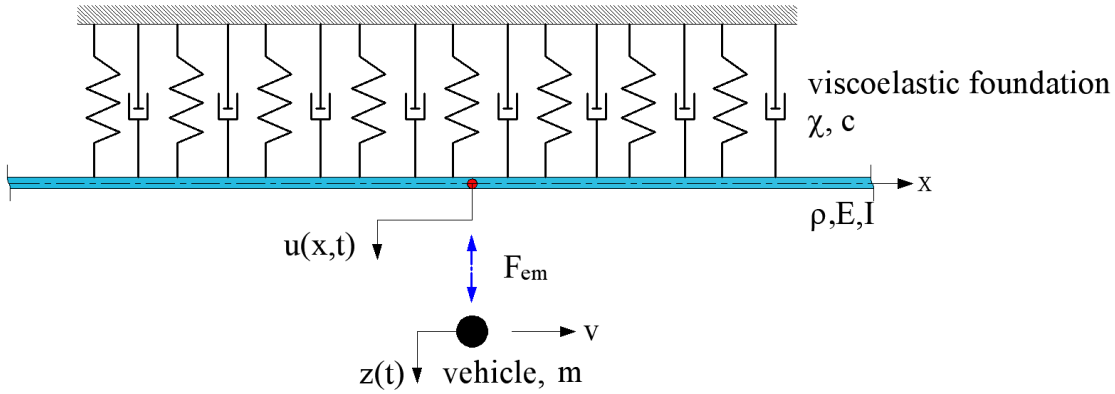


*Figure 3. 1 Model of EMS levitation system and reference frame definition. The beam and vehicle share the same reference point in the vertical direction which is denoted as a red dot.*

One can now write the governing system of equations of motion as

$$\begin{cases} \rho\ddot{u} + EIu'''' + c\dot{u} + \chi u = F_{em}\delta(x - vt) \\ m\ddot{z} = mg - F_{em} \\ F_{em} = \operatorname{sgn}(z-u)\dfrac{\mu_0 N^2 A_m}{4}\dfrac{i^2}{(z-u)^2} \\ \dot{i} = \dfrac{z-u}{2C}[U - iR + 2C\dfrac{i}{(z-u)^2}(\dot{z}-\dot{u})] \end{cases} \tag{3.1}$$

Where $z(t)$ and $u(x,t)$ are the vertical displacements of the vehicle and the beam respectively, $m$ is the mass of vehicle, $\rho$ and $EI$ are the mass per unit length and the bending stiffness of the beam, $c$ and $\chi$ are the viscosity and stiffness of the foundation per unit length, $v$ is the velocity of the vehicle, $\delta(\cdots)$ is the Dirac delta

function, $F_{em}$ is the electromagnetic force, $\mathrm{sgn}(z-u)$ refers to the sign of levitation air gap and ensures the electromagnetic force is always in attraction so that in unrealistic case the vehicle could pass through the rail, $i$ is the electric current flowing through the coil, $U$ is the voltage of control system, $R$ is the total resistance of the coil.

As shown in eq. 3.1, the non-linear dependency of the electromagnetic force on the levitation air gap $\delta$ and the electric current $i$ is taken from available literatures [16-22], where $\mu_0$ is the permeability in vacuum, $N$ is the number of turns of the coil, $A_m$ is the area of the magnetic pole of the electromagnet. For the sake of simplicity all constant parameters are combined in a generic constant $C=\frac{\mu_0 N^2 A_m}{4}$. Furthermore, the ordinary differential equation of current is derived from eq. 3.2 following the Kirchhoff's law of total voltage which is explained in section 2.3 [16-22].

$$U = iR + 2C\frac{\dot{i}}{\delta} - 2C\frac{i}{\delta^2}\dot{\delta} \tag{3.2}$$

The levitation air gap $\delta$ is defined as the difference between the displacement of the vehicle and that of beam:

$$\delta = z - u \tag{3.3}$$

This project is aimed at studying dynamic problems by both non-linear simulations and analytical linearized approximations through MATLAB. Numerical values of all the parameters defined above to describe the model are collected in the following table (*Table 3. 1*), where the value of reference mass $M$ is the summation of mass of vehicle (10 meters long) and mass of one magnet [8].

| **Parameter** | **Value** | **Unit** |
|---|---|---|
| $M$ | 10150 | kg |
| $\rho$ | 268.3 | kg/m |
| $EI$ | $6.42\cdot10^{6}$ | N m$^2$ |
| $c$ | $1.495\cdot10^{4}$ | kg/(m s) |
| $\chi$ | $8.33\cdot10^{7}$ | kg/(m s$^2$) |
| $g$ | 9.81 | m/s$^2$ |
| $R$ | 9.71 | Ω |
| $\mu_0$ | $4\pi\cdot10^{-7}$ | T m/A |
| $N$ | 800 | – |
| $A_m$ | 0.25 | m$^2$ |
| $C$ | 0.0503 | T m$^3$/A |
| $\delta_0$ (Target air gap) | 0.015 | m |
| $v$ (When no special statement) | 300 | m/s |
| $v_{crit}$ (Critical velocity) | 415.19 | m/s |

*Table 3. 1 Input numerical values of model parameters*

# 4. Numerical Non-Linear Simulations

This chapter focuses on reveling the effects of EMS system on stability of vehicle-beam coupled system by numerical simulations. Along this line, here firstly explain why and how to apply the numerical method, secondly, validate this method by comparing the outcomes of simple simulations under varying values of mass, thirdly, search for appropriate combinations of PD control to stabilize the system with fixed mass and velocity, lastly, study the stability of the system to find the stable region of velocity for fixed mass, $K_p$ and $K_d$, draw the relationship between different governing parameters, e.g., velocity versus $K_p$, which is capable of keeping the system stable.

## 4.1.Idea of numerical method

It's nearly impossible to find analytical solution of eq. 3.1 due to non-linearity and partial differentiation. Thus, the basic idea is to find the numerical solution. To do this, one can first put the original system into moving reference frame under the following assumptions

$$\xi = x - vt, \tau = t \tag{4.1}$$

Then one can rewrite eq. 3.1 as

$$\begin{cases} \rho(v^2 u'' - 2v\dot{u}' + \ddot{u}) + EIu'''' + c(-vu' + \dot{u}) + \chi u = F_{em}\delta(\xi) \\ m\ddot{z} = mg - F_{em} \\ F_{em} = \operatorname{sgn}(z-u)C\dfrac{i^2}{(z-u)^2} \\ \dot{i} = \dfrac{z-u}{2C}[U - iR + 2C\dfrac{i}{(z-u)^2}(\dot{z} - \dot{u})] \end{cases} \tag{4.2}$$

Where $u$ is now a function of $\xi$ and $\tau$. Afterward, one can rewrite the equation of motion of beam as well as that of vehicle in form of convolution integral as

$$\begin{cases} u(\xi = 0, t) = \int_0^t g_{EB}(t-\tau)F_{em}(\tau)d\tau + u_f(t) \\ z(t) = \dfrac{gt^2}{2} - \int_0^t g_m(t-\tau)F_{em}(\tau)d\tau + z_f(t) \end{cases} \tag{4.3}$$

Where $g_{EB}(t)$ and $g_m(t)$ are the Green's functions of beam and vehicle in the moving reference frame evaluated at $\xi = 0$, respectively. $u_f(t)$ and $z_f(t)$ are free-vibration parts of beam and vehicle which stand for initial conditions. As the air gap is equal to the difference of displacements of the vehicle and the beam right above the vehicle, the deflection of the beam should be taken at $\xi = 0$.

The Green's function of vehicle is easy to derive and here the result is directly given by

$$g_m(t) = \frac{t}{m} \tag{4.4}$$

### *4.1.1. Green's function of beam*

Now one should determine the Green's function of beam numerically, and solve for free-vibrations with given initial conditions. The equation of motion of beam is taken out from eq. 4.2 separately for ease of citation.

$$\rho(v^2u'' - 2v\dot{u}' + \ddot{u}) + EIu'''' + c(-vu' + \dot{u}) + \chi u = F_{em}\delta(\xi) \tag{4.5}$$

To ensure the outcome is correct., here two different ways are used to obtain the Green's function of beam.

**1. Contour integration from Fourier domain**

Firstly, one can solve eq. 4.5 by using the Laplace transform with respect to $\tau$ and the Fourier transform with respect to $\xi$ . These transforms are

$$V(\xi, s) = \int_0^\infty u(\xi, \tau)e^{(-s\tau)}d\tau \,,\; W(k, s) = \int_{-\infty}^\infty V(\xi, s)e^{(-ik\xi)}d\xi$$

And after applying them to eq. 4.5 brings about

$$(k^4 - \frac{\rho v^2}{EI}k^2 - \frac{(2i\rho vs + icv)}{EI}k + \frac{\rho s^2 + \chi + cs}{EI})W(k, s) = \frac{F_{em}(s)}{EI} \tag{4.6}$$

Where $F_{em}(s)$ is the electromagnetic force in the Laplace domain, trivial initial conditions $u(\xi, 0) = \dot{u}(\xi, 0) = 0$ are taken. Now applying inverse Fourier transform to obtain the solution in the Laplace domain yields

$$V(\xi, s) = \frac{F_{em}(s)}{2\pi EI}\int_{-\infty}^\infty \frac{e^{ik\xi}}{D(k, s)}dk \tag{4.7}$$

Where $D(k, s) = k^4 - \frac{\rho v^2}{EI}k^2 - \frac{(2i\rho vs + icv)}{EI}k + \frac{\rho s^2 + \chi + cs}{EI}$ . One could rewrite eq. 4.7 as

$$V(\xi, s) = F_{em}(s)g_{EB}(\xi, s) \tag{4.8}$$

Where $g_{EB}(\xi, s) = \frac{1}{2\pi EI}\int_{-\infty}^\infty \frac{e^{ik\xi}}{D(k, s)}dk$ is the Green's function of the beam in Laplace domain and the integral part can be solved by using contour integration method. This results in the following expression

$$\begin{cases} g_{EB1}(\xi,s)=\dfrac{i}{EI}\sum_{n}\lim_{k\to k_n}\dfrac{(k-k_n)}{(k-k_1)(k-k_2)(k-k_3)(k-k_4)},\xi>0 \\ g_{EB2}(\xi,s)=-\dfrac{i}{EI}\sum_{m}\lim_{k\to k_m}\dfrac{(k-k_m)}{(k-k_1)(k-k_2)(k-k_3)(k-k_4)},\xi<0 \end{cases} \tag{4.9}$$

Where $k_n$ and $k_m$ are the roots of the equation $D(k,i\omega)=0$ which possess a positive imaginary part and negative imaginary part, respectively. This can be done numerically via MATLAB.

The results of the absolute value of Green's function evaluated at $\xi=0$ in the Laplace domain are shown below (*Figure 4. 1*)

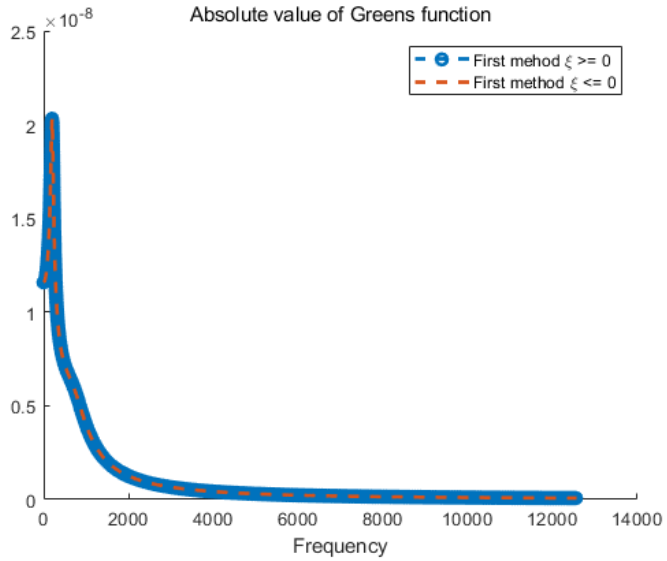


*Figure 4. 1 Absolute value of Green's function evaluated at* $\xi=0$ *in the Laplace domain by contour integration*

## 2. Superposition of wave modes in Laplace domain

Secondly, one could solve eq. 4.5 by using only the Laplace transform with respect to $\tau$, it yields

$$V''''+\frac{\rho}{EI}v^2V''-(\frac{\rho}{EI}2vs+\frac{c}{EI}v)V'+(\frac{\rho}{EI}s^2+\frac{c}{EI}s+\frac{\chi}{EI})V=\frac{F_{em}(s)}{EI}\delta(\xi) \tag{4.10}$$

It is advantageous to divide the system into two domains: domain 1 represents the system behind the load ($\xi<0$) and domain 2 in front of the load ($\xi>0$). Eq. 4.5 could be rewritten as

$$\begin{cases} V_1''''+\dfrac{\rho}{EI}v^2V_1''-(\dfrac{\rho}{EI}2vs+\dfrac{c}{EI}v)V_1'+(\dfrac{\rho}{EI}s^2+\dfrac{c}{EI}s+\dfrac{\chi}{EI})V_1=0,\xi<0 \\ V_2''''+\dfrac{\rho}{EI}v^2V_2''-(\dfrac{\rho}{EI}2vs+\dfrac{c}{EI}v)V_2'+(\dfrac{\rho}{EI}s^2+\dfrac{c}{EI}s+\dfrac{\chi}{EI})V_2=0,\xi>0 \end{cases} \tag{4.11}$$

The interface conditions should be imposed which represent the continuity in displacements and slope between the two domains as well as the equilibrium of bending moment and shear force, respectively. They may be expressed as follows

$$\begin{cases} V_1 = V_2 \\ V_1' = V_2' \\ V_1'' = V_2'' \\ V_2''' - V_1''' = \dfrac{1}{EI} \end{cases}, \xi = 0 \tag{4.12}$$

Where $F_{em}(s)$ is now regarded as a unit force since the Green's function is the key point here.

Then assume the solutions of eq. 4.11 to be in the form of harmonic waves

$$\begin{aligned} V_1 &= \sum A e^{-ik\xi} \\ V_2 &= \sum B e^{-ik\xi} \end{aligned} \tag{4.13}$$

Where $A_n$ and $B_n$ represent the amplitudes of the harmonic waves and $k$ represents the wave number of the harmonic waves. Substituting this assumed form of solutions into eq. 4.11. one obtains

$$\begin{aligned} &(k^4 - \frac{\rho v^2}{EI}k^2 + \frac{(2i\rho vs + icv)}{EI}k + \frac{\rho s^2 + \chi + cs}{EI}) A_n e^{-ik\xi} = 0, \\ &(k^4 - \frac{\rho v^2}{EI}k^2 + \frac{(2i\rho vs + icv)}{EI}k + \frac{\rho s^2 + \chi + cs}{EI}) B_n e^{-ik\xi} = 0 \end{aligned} \tag{4.14}$$

The exponent cannot be zero for all positions in space and we are not interested in the trivial solution, namely $A_n = B_n = 0$. Thus, in order to satisfy eq. 4.14, the expression in the parenthesis must be zero and reads

$$k^4 - \frac{\rho v^2}{EI}k^2 + \frac{(2i\rho vs + icv)}{EI}k + \frac{\rho s^2 + \chi + cs}{EI} = 0 \tag{4.15}$$

The solutions can be found numerically, namely $k_1, k_2, k_3, k_4$, for each value of $s$. Considering the solutions must vanish as $\xi \to \pm\infty$, the expressions of displacements of beam in Laplace domain can be written as follows

$$\begin{cases} V_1 = A_1 e^{-ik_1\xi} + A_2 e^{-ik_2\xi}, \xi < 0 \\ V_2 = B_3 e^{-ik_3\xi} + B_4 e^{-ik_4\xi}, \xi > 0 \end{cases} \tag{4.16}$$

Where $k_1$ and $k_2$ have positive imaginary parts while $k_3$ and $k_4$ have negative imaginary parts. Now one could plot the absolute value of Green's function in Laplace domain and compare with the one obtained in first method, see *Figure 4. 2* below.

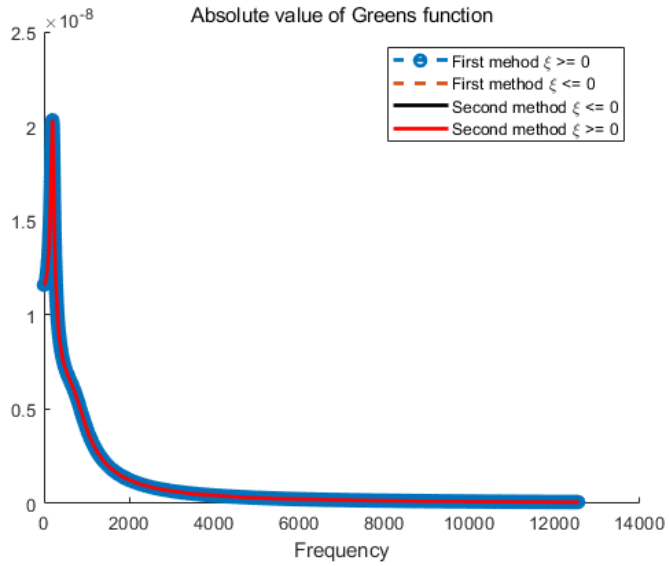


*Figure 4. 2 Comparison of absolute value of Green's function evaluated at* $\xi = 0$ *from both methods in the Laplace domain*

It can be told that the outcomes of Green's function obtained from different ways fully overlap each other, which could be regard as a signal to say the Green's function is correct.

In this case, one could further derive the Green's function in time domain by using trapezoidal function in MATLAB. The outcomes are illustrated in *Figure 4. 3*

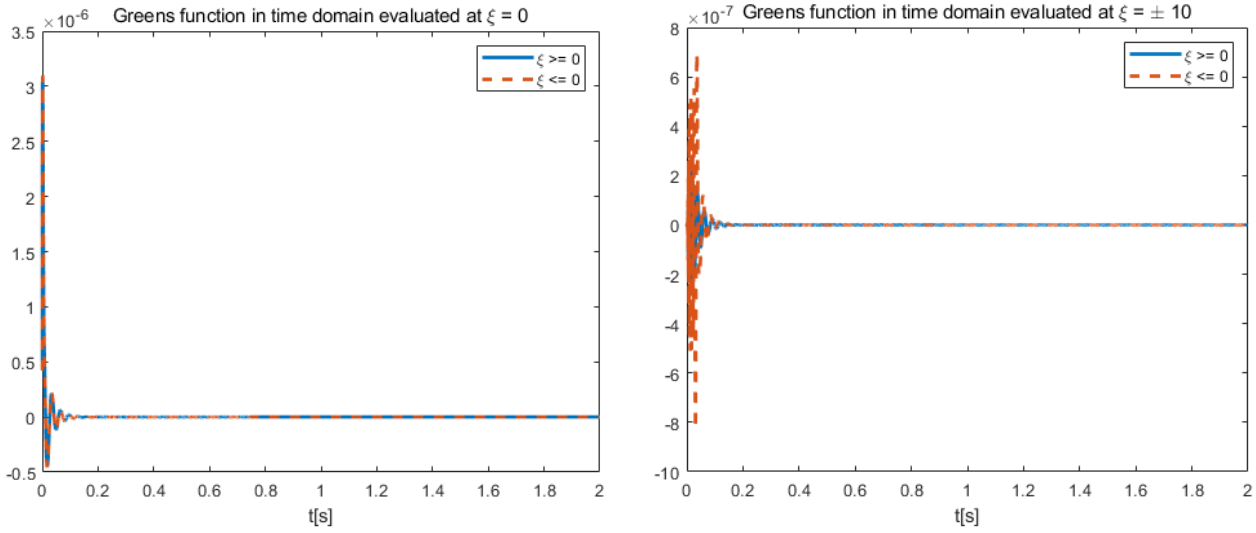


*Figure 4. 3 Green's function in time domain. It is evaluated at* $\xi = 0$ on the right and *at* $\xi = \pm 10$ on the Left

It can be concluded that the Green's function of the beam in the moving reference frame is continuous at $\xi = 0$ and asymmetric with respect to $\xi = 0$. The latter is reasonable as eq. 4.15 is an odd function so that the roots are not symmetric in the complex plane.

To validate the Green's function, here also plot the displacement of the beam (*Figure 4. 4*) under a moving constant load ( $F_{em} = mg$ ) with trivial initial conditions and compare the steady-state with that obtained analytically [27].

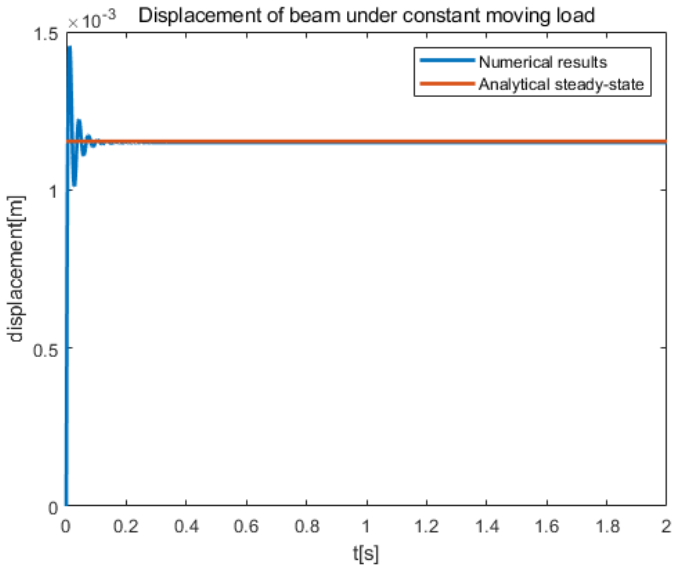


*Figure 4. 4 Displacement of beam obtained by Green's function and analytical steady-state response*

As can be seen, the two results are different initially since the blue one is the transient response of the system while the red one is the steady-state response. With time goes by the system steps into steady-state (horizontal part in *Figure 4. 4*) and the displacements of beam obtained numerically almost overlap with the analytical results which means the Green's function is correct.

### *4.1.2. Free-vibrations of beam and vehicle*

If one uses Green's function only to determine the response of the system, then no information about initial conditions will be included as Green's function is based on zero initial condition. In the following research, to study the behavior of the system around the equilibrium point, initial perturbations of beam and vehicle from steady-state position are required to impose which means one should add another part of vibrations to take the initial conditions into account, namely free-vibration.

The free-vibration part of vehicle is easy to derive and it reads

$$z_f = z_0 + v_{z0}t \tag{4.17}$$

Where $z_0$ and $v_{z0}$ are the initial displacement and velocity respectively.

For the solution of free-vibration part of beam, one should first transform eq. 4.5 into Laplace domain with zero external force and non-zero initial conditions, it follows

$$V'''' + \frac{\rho}{EI}v^2V'' - (\frac{\rho}{EI}2vs + \frac{c}{EI}v)V' + (\frac{\rho}{EI}s^2 + \frac{c}{EI}s + \frac{\chi}{EI})V = \frac{\rho}{EI}(su_0 + v_{u0}) + \frac{c}{EI}u_0 - 2v\frac{\rho}{EI}u_0' \tag{4.18}$$

Where $u_0(\xi)$ and $v_{u0}(\xi)$ are the initial displacement and velocity of the beam in the moving reference frame, $u_0'(\xi)$ stands for the first space derivative of initial displacement. Here the steady-state solution of the beam under constant moving load ( $F_{em} = mg$ ) is chosen as the initial conditions, of which the derivation process is explained in detail in many available literatures [27].

Then split eq. 4.18 into the superposition of two parts, they read

$$\begin{cases} V_p'''' + \frac{\rho}{EI}v^2 V_p'' - (\frac{\rho}{EI}2vs + \frac{c}{EI}v)V_p' + (\frac{\rho}{EI}s^2 + \frac{c}{EI}s + \frac{\chi}{EI})V_p = \frac{\rho}{EI}(su_0 + v_{u0}) + \frac{c}{EI}u_0 - 2v\frac{\rho}{EI}u_0' \\ V_h'''' + \frac{\rho}{EI}v^2 V_h'' - (\frac{\rho}{EI}2vs + \frac{c}{EI}v)V_h' + (\frac{\rho}{EI}s^2 + \frac{c}{EI}s + \frac{\chi}{EI})V_h = 0 \end{cases} \tag{4.19}$$

Where $V_p$ and $V_h$ stand for particular solution and homogeneous solution of free-vibration part of beam, respectively. Now one could solve eq. 4.19 with known initial conditions and interface conditions at the point of load, they could be written as following steps

1. Assume the solutions to be in the form of harmonic waves

$$\begin{cases} V_p = \sum A_p e^{-ik_p\xi} \\ V_h = \sum A_h e^{-ik_h\xi} \\ u_0 = \sum B e^{-ik_p\xi} \\ v_{u0} = 0 \end{cases} \tag{4.20}$$

Where $B_{1,2,3,4}$ and $k_{p1,p2,p3,p4}$ are known constants, $A_p$ and $A_h$ are amplitudes of particular solution and homogenous solution respectively, $k_h$ is wavenumber of homogenous solution.

2. Solve for $A_p$ by substituting eq. 4.20 into eq. 4.19

$$\begin{cases} V_{p1}'''' + \frac{\rho}{EI}v^2 V_{p1}'' - (\frac{\rho}{EI}2vs + \frac{c}{EI}v)V_{p1}' + (\frac{\rho}{EI}s^2 + \frac{c}{EI}s + \frac{\chi}{EI})V_{p1} = \frac{\rho}{EI}su_{01} + \frac{c}{EI}u_{01} - 2v\frac{\rho}{EI}u_{01}', \xi < 0 \\ V_{p2}'''' + \frac{\rho}{EI}v^2 V_{p2}'' - (\frac{\rho}{EI}2vs + \frac{c}{EI}v)V_{p2}' + (\frac{\rho}{EI}s^2 + \frac{c}{EI}s + \frac{\chi}{EI})V_{p2} = \frac{\rho}{EI}su_{02} + \frac{c}{EI}u_{02} - 2v\frac{\rho}{EI}u_{02}', \xi > 0 \end{cases} \tag{4.21}$$

Where $V_{p1} = A_{p1}e^{-ik_{p1}\xi} + A_{p2}e^{-ik_{p2}\xi}$ and $u_{01} = B_1 e^{-ik_{p1}\xi} + B_2 e^{-ik_{p2}\xi}$, $V_{p2} = A_{p3}e^{-ik_{p3}\xi} + A_{p4}e^{-ik_{p4}\xi}$ and $u_{02} = B_3 e^{-ik_{p3}\xi} + B_4 e^{-ik_{p4}\xi}$, $k_{p1}$ and $k_{p2}$ are roots with a positive imaginary part, $k_{p3}$ and $k_{p4}$ are roots with a negative imaginary part.

3. Solve for wavenumber $k_h$

$$k_h^4 - \frac{\rho v^2}{EI}k_h^2 + \frac{(2i\rho vs + icv)}{EI}k_h + \frac{\rho s^2 + \chi + cs}{EI} = 0 \tag{4.22}$$

Eq. 4.22 has 4 roots, say that $k_{h1}$ and $k_{h2}$ are roots with a positive imaginary part, $k_{h3}$ and $k_{h4}$ are roots with a negative imaginary part.

4. Solve for $A_h$ by imposing interface conditions

$$\begin{cases} V_1 = V_2 \\ V_1' = V_2' \\ V_1'' = V_2'' \\ V_2''' - V_1''' = 0 \end{cases}, \xi = 0 \tag{4.23}$$

Where $V_1 = V_{p1} + V_{h1}$ and $V_2 = V_{p2} + V_{h2}$.

Afterwards, the free-vibration part of beam in Laplace domain is obtained and one needs to use trapezoidal function to transform the outcome into time domain. The shape of free-vibration of beam under given initial conditions at $t = 0$ is shown below (*Figure 4. 5*)

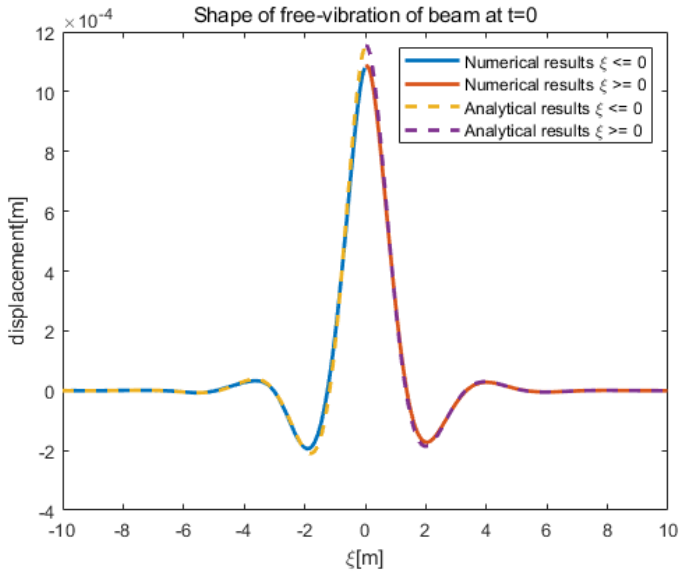


*Figure 4. 5 Shape of free-vibration of beam at t=0*

To corroborate $u_f$ , here both the numerical outcomes (solid line) and the analytical steady-state solution (dash line) are illustrated in *Figure 4. 5* for the sake of comparison. It can be observed that small errors exist and this is due to the energy cannot be all captured by the frequency range set ( $f_{\max} = 2000\,\text{Hz}$ ), if one increases the maximum frequency, the error will decrease. Here the error is about 6% and it's acceptable, $u_f$ is correct.

### *4.1.3. Basic assumption of numerical method*

As eq. 4.3 shows, the displacement of beam and vehicle are now expressed in the form of convolution integral. Now assume the integral can be solved by using trapezoidal rule if the interval is quite small

$$\int_a^b f(x)dx \approx (b-a)\cdot\frac{1}{2}(f(a)+f(b)) \tag{4.24}$$

Then rewrite integral terms of eq. 4.3 to be the summation of infinitely many integrals as

$$\begin{cases} u(t_N) = \sum_{n=1}^{N} \int_{t_{n-1}}^{t_n} g_{EB}(t-\tau) F_{em}(\tau) d\tau + u_f(t_N) \\ z(t_N) = \frac{g t_N^2}{2} - \sum_{n=1}^{N} \int_{t_{n-1}}^{t_n} g_m(t-\tau) F_{em}(\tau) d\tau + z_f(t_N) \end{cases} \tag{4.25}$$

Where $t_n - t_{n-1} = \delta t$ and $\delta t$ is small enough. By applying eq. 4.24 to eq. 4.25 results in

$$\begin{cases} u(t_N) = u_f(t_N) + \sum_{n=1}^{N} \frac{dt}{2} (g_{EB}(t-t_n) F_{em}(t_n) + g_{EB}(t-t_{n-1}) F_{em}(t_{n-1})) \\ z(t_N) = \frac{g t_N^2}{2} + z_f(t_N) - \sum_{n=1}^{N} \frac{dt}{2} (g_m(t-t_n) F_{em}(t_n) + g_m(t-t_{n-1}) F_{em}(t_{n-1})) \end{cases} \tag{4.26}$$

Where $g_{EB}, g_m, u_f, z_f$ are already obtained numerically (section 4.1.1), $F_{em}(t_0), F_{em}(t_1), \ldots, F_{em}(t_{N-1})$ are referred as historical terms and are known, $F_{em}(t_N)$ is called instantaneous term and remain unsolved.

Eq. 4.26 is a system of algebraic equations and solvable when it's combined with the equation of electromagnetic force at each time step ( $n = 1, 2, \ldots N$ ) as the latter is an explicit function of $u$ and $z$ .

$$F_{em}(t_N) = \mathrm{sgn}(\delta(t_N)) C \frac{i^2(t_N)}{(z(t_N) - u(t_N))^2} \tag{4.27}$$

The electric current is expressed in an ordinary differential equation as shown in eq. 4.2 and the whole system ( $u(t_N)$ , $z(t_N)$ , $F_{em}(t_N)$ , $i(t_N)$ ) could be solved by time-stepping scheme (For loop) in MATLAB with finite difference method or ODE45 if initial conditions are given.

## 4.2.Validation of numerical model

To verify the aforementioned numerical method, here a simple system (*Figure 4. 6*) is created in which the vehicle is moving uniformly on the beam and they are connected by a linear spring. What's more, a constant force is imposed on the vehicle while the gravity is neglected.

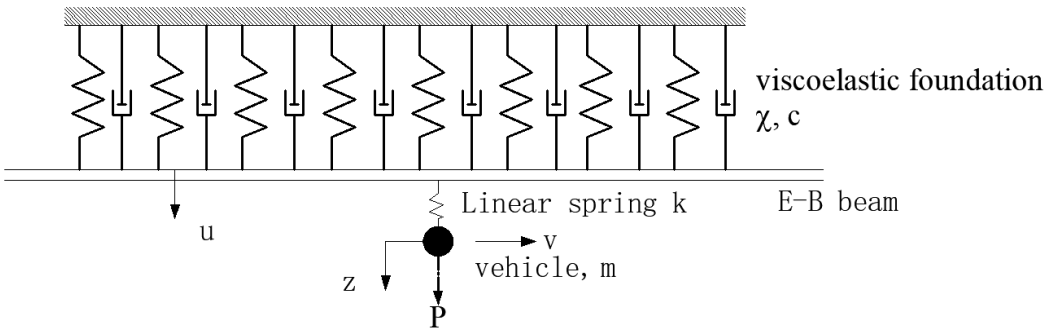


*Figure 4. 6 Simplified linear mechanical system*

Where $k = 100000000$ N/m is the stiffness of the spring, $P$ is a constant force acting on the vehicle. Now one can imagine that if the mass of the vehicle $m$ is small enough, then the effective force acting on the beam is equal to $P$. It can be easily derived from the equation of motion of vehicle as shown below

$$m\ddot{z} = P - k\delta \tag{4.28}$$

If $m = 0$, $P - k\delta = 0$. We verify that with the decrease of mass, the displacement of beam will converge to the one under moving constant load $P$ (which is already discussed in section 4.1.1).

Then one is supposed to use eq. 4.26 to solve for the response of the system but combined with a different linear force equation. The displacements of beam are illustrated in detail in *Figure 4. 7* for different value of $m$.

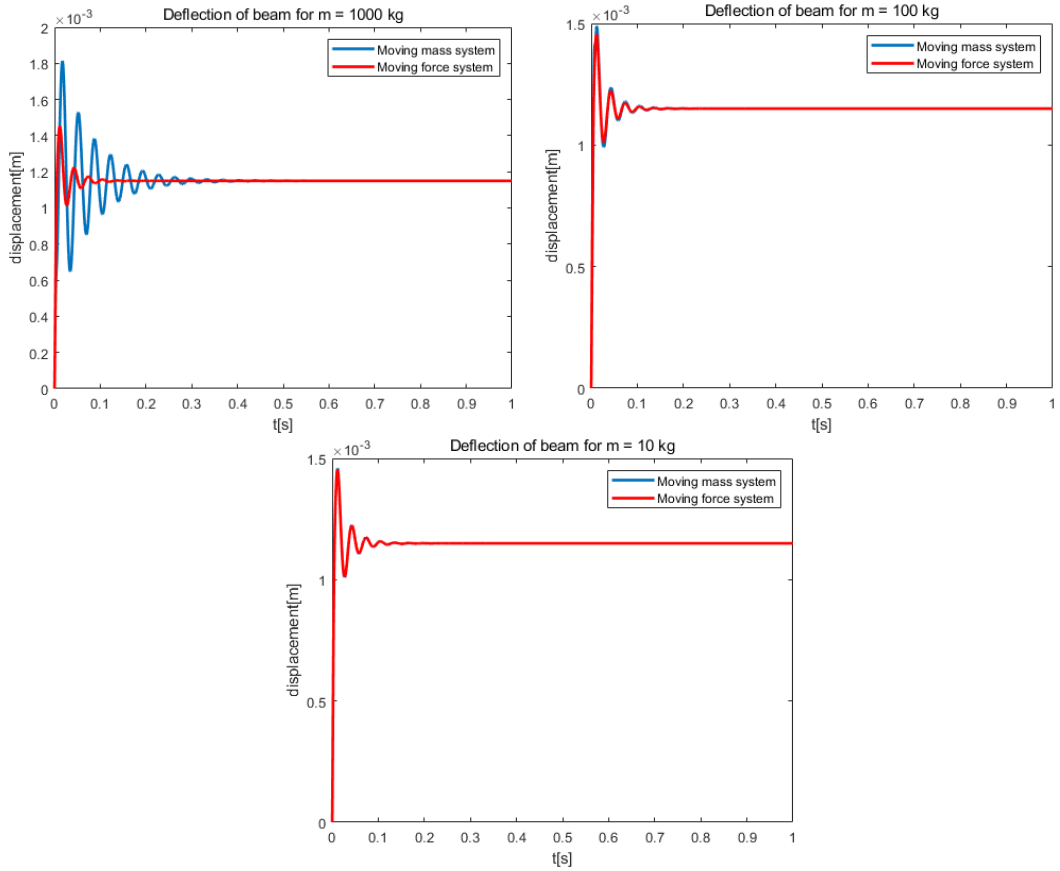


*Figure 4. 7 Deflections of beam under decreasing value of the vehicle mass. The blue solid line represents the displacement in the moving mass system, the red one represents the displacement in the moving force system.*

As can be seen from *Figure 4. 7*, when the mass of vehicle is quite small ($m = 10$ kg), the deflections of beam coincide with the one under moving constant force, at each time moment. This limit case verifies the numerical model.

## 4.3.Stability study of EMS vehicle-beam coupled system[1]

[1] All results obtained in this section are based on the wrong differential equation of current (eq. 4.31) where the sign of last term is negative. However, this will only influence the exact quantities and the quality is not affected.

As the numerical tool can only tell the results of simulations, untill now, no information is obtained about the nature of stability of this system (eigenvalues, etc.). Thus, this section focuses on imposing different closed-loop control systems (basically PD) based on available analytical study of simplified 2 degrees of freedom system [8] to see how the more realistic and complex model (infinite degrees of freedom) will behave, then some sets of control systems are chosen under which the vehicle-beam coupled system would show representative characteristics to draw the combined effects of EMS system and one-dimensional guideway.

### *4.3.1. Appropriate closed-loop PD control*

As mentioned in section 2.4, for this control the input is the error defined as $e = z - u - \delta_0$ and the output is the voltage $U$ . Thus, the control loop can be expressed as

$$U = K_p e + K_d \dot{e} + U_0 = K_p(\delta - \delta_0) + K_d \dot{\delta} + U_0 \tag{4.29}$$

Where $U_0$ is the initial voltage and the value can be calculated as follows

$$C\frac{i_0^2}{\delta_0^2} = mg \xrightarrow{i_0 = \frac{U_0}{R}} C\frac{U_0^2}{R^2\delta_0^2} = mg \rightarrow U_0 = R\delta_0\sqrt{\frac{mg}{C}} \tag{4.30}$$

In this case, the expression of electric current becomes

$$\dot{i} = \frac{\delta}{2C}[K_p(\delta - \delta_0) + K_d\dot{\delta} + U_0 - iR + 2C\frac{i}{\delta^2}\dot{\delta}] \tag{4.31}$$

To avoid the unrealistic negative current, the switch on/off control is also added into the system which will cut off the power when the output of eq. 4.31 is negative.

As the main purpose of this thesis is to reveal the deficiencies of the simplified two degrees of freedom model and show the actual effects of EMS on stability under varying velocity of vehicle, here the values of control gains ( $K_p$ and $K_d$ ) are chosen on the premise of stabilizing the system in simplified model (*Figure 4. 8*).

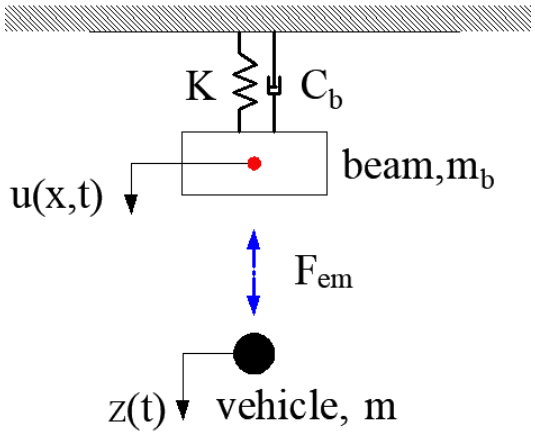


*Figure 4. 8 Simplified two degrees of freedom model. The beam and vehicle share the same reference point in the vertical direction which is denoted as a red dot.*

The beam is now regarded as a point mass, $m_b$ and $K$ are dynamic mass and stiffness respectively, they can be obtained by solving $abs((m_b s^2 + C_b s + K)^{-1}) \approx abs(g_{EB}(s))$ where $g_{EB}(s)$ is the Green's function of beam in Laplace domain when the horizontal velocity of vehicle is 0, and $C_b = 0.05 \cdot 2\sqrt{Km_b}$ .

Three sets of $K_p$ and $K_d$ combinations are chosen and they are 1. $K_p = 16000, K_d = 24000$ ; 2. $K_p = 60000, K_d = 100000$ ; 3. $K_p = 600000, K_d = 100000$ . The first two can stabilize the system in simplified model while the third leads to instability. The displacements of the beam and vehicle in simplified two degrees of freedom system for these three groups of control gains are illustrated in *Figure 4. 9*, where the initial perturbations are the same as case 1 in the following.

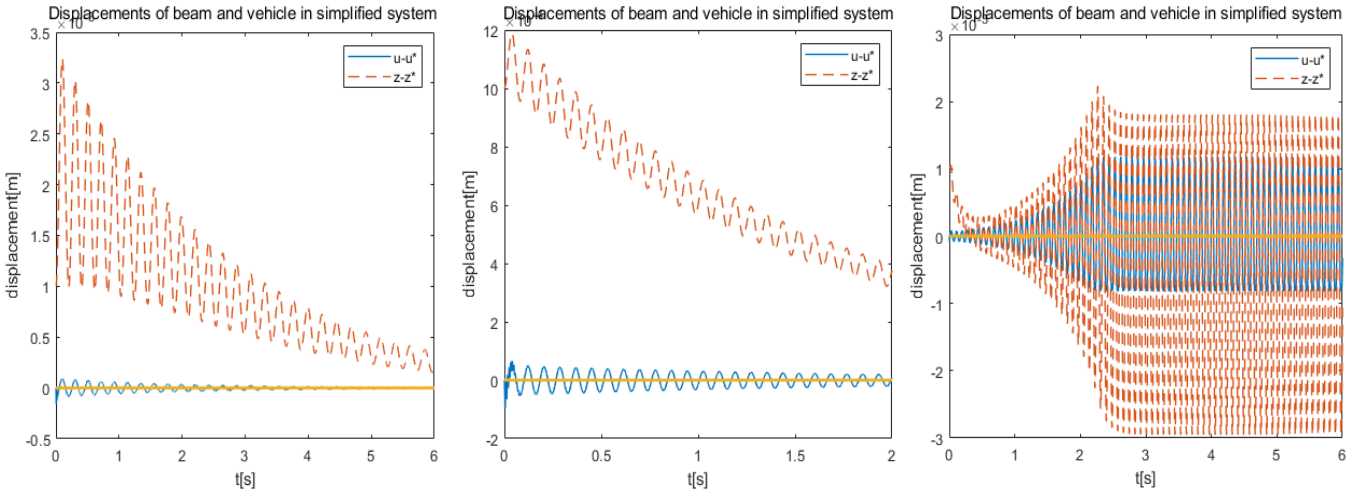


*Figure 4. 9 The displacements of beam and vehicle in simplified system for three different sets of control gains (left:* $K_p = 16000, K_d = 24000$ *; middle:* $K_p = 60000, K_d = 100000$ *; right:* $K_p = 600000, K_d = 100000$ *)*

Below, the response (the displacements of beam and vehicle, electric current and electromagnetic force) of the system $\{z, u, i, F_{em}\}$ in one-dimensional model is presented in time domain for two sets of control gains (left and right of *Figure 4. 9*) and the phase portrait of the vehicle for different initial conditions is also illustrated. To be noted, the displacement of beam $u$ in all subsequent studies is evaluated at $\xi = 0$ .

**Case 1**. $K_p = 16000, K_d = 24000$ , $v = 300$ [**m/s**] (*Figure 4. 10*)

Here the initial perturbation is imposed on the position and velocity of vehicle and they read $z(0) - z^* = 0.001$ and $v_{zini} = 0.01$ , where $z^*$ and $v_{zini}$ are the steady-state position and initial vertical velocity of vehicle respectively, $u^*$ is the steady-state displacement of beam under moving constant load $F_{em} = mg$ , $z^* = u^* + \delta_0$ ; the initial conditions of other parameters are $u(0) = u^*$ , $v_u(0) = 0$ , and $i(0) = \frac{U_0}{R}$ (these keep unchanged in the following research)

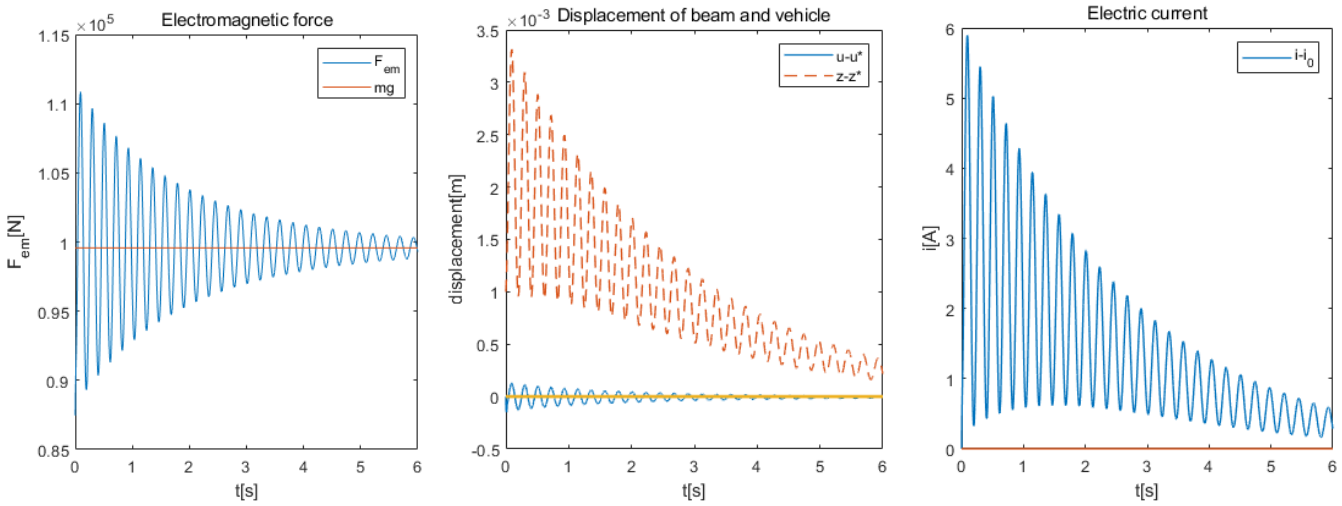


*Figure 4. 10 Non-linear simulations of the response of the system in time domain for* $K_p = 16000$ *and* $K_d = 24000$

It can be easily observed from *Figure 4. 10* that the system is stable around the equilibrium point (steady-state position) as the force, displacement, and current all converge to steady-state value. The decaying trend of electric current is similar to that of vehicle's displacements.

Moreover, the outcomes are in accordance to the ones of simplified model which means that it might be safe to use simplified model to predict the stability of the system at subcritical velocity.

The phase portrait of the vehicle in this case for different initial perturbations is shown in *Figure 4. 11*, where the red dot represents the starting point, $z_{ini} = z(0) - z^*$, $v_{zini}$ is the initial vertical velocity. One can tell that the system becomes unstable when the initial velocity is relatively large or the initial perturbation is negative (green line in *Figure 4. 11*).

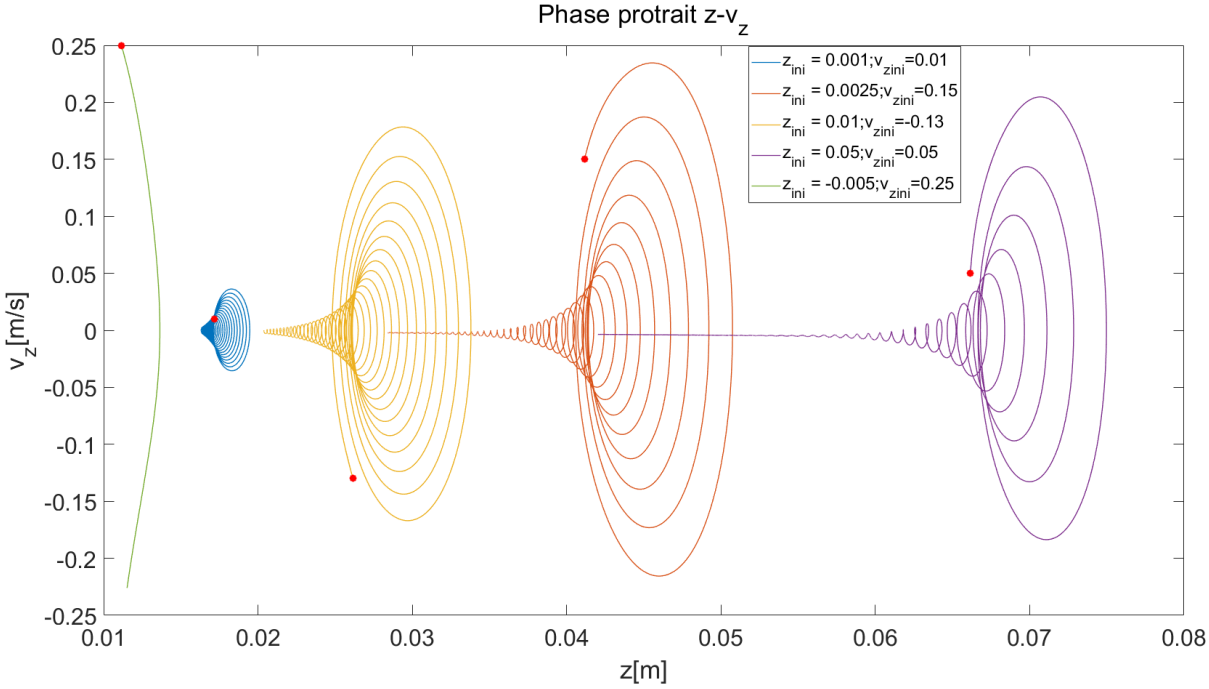


*Figure 4. 11 Phase portrait of the vehicle* $z - \dot{z}$ *for different initial perturbations*

**Case 2**. $K_p = 600000, K_d = 100000$, $v = 300$ [m/s] (*Figure 4. 12*) & $v = 350$ [m/s] (*Figure 4. 13*)

Here the initial perturbation is the same as that in case 1. The response of different variables of the system is shown in *Figure 4. 12*.

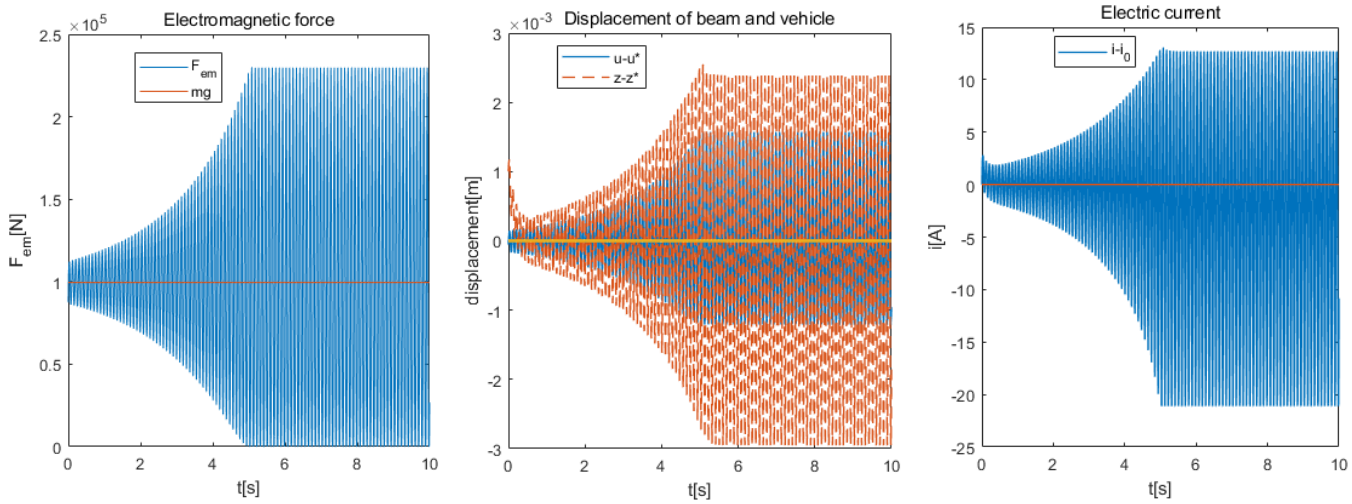


*Figure 4. 12 Non-linear simulations of the response of the system in time domain for* $K_p = 600000$ *and* $K_d = 100000$, $v = 300$ [m/s]

The outcomes are still in accordance to the ones of simplified model as a stable limit cycle appears and the equilibrium point is unstable, does this mean that the simplified model is sufficient? The answer is no. As the influence of beam on stability are still unknown, one could try another velocity of the vehicle, e.g., $v = 350$ [m/s], to see the how the system will behave (*Figure 4. 13*).

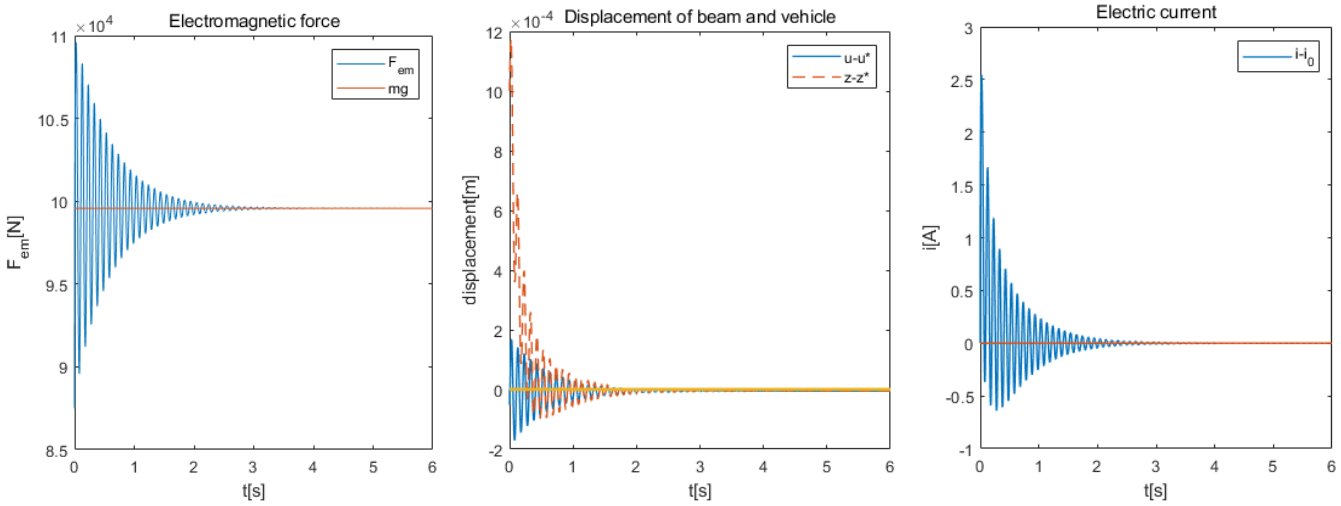


*Figure 4. 13 Non-linear simulations of the response of the system in time domain for* $K_p = 600000, K_d = 100000$, $v = 350$ [m/s]

One can see that for a different (larger) velocity the previous unstable system becomes stable, which is counter-intuitive. This confirms that the horizontal velocity plays an important role in the stability of EMS system and the following sections will try to elaborate the relationship of velocity and other parameters to maintain the stability of the system.

It would be good to also plot the phase portrait of the vehicle for this case (*Figure 4. 14*) and compare with that of case 1

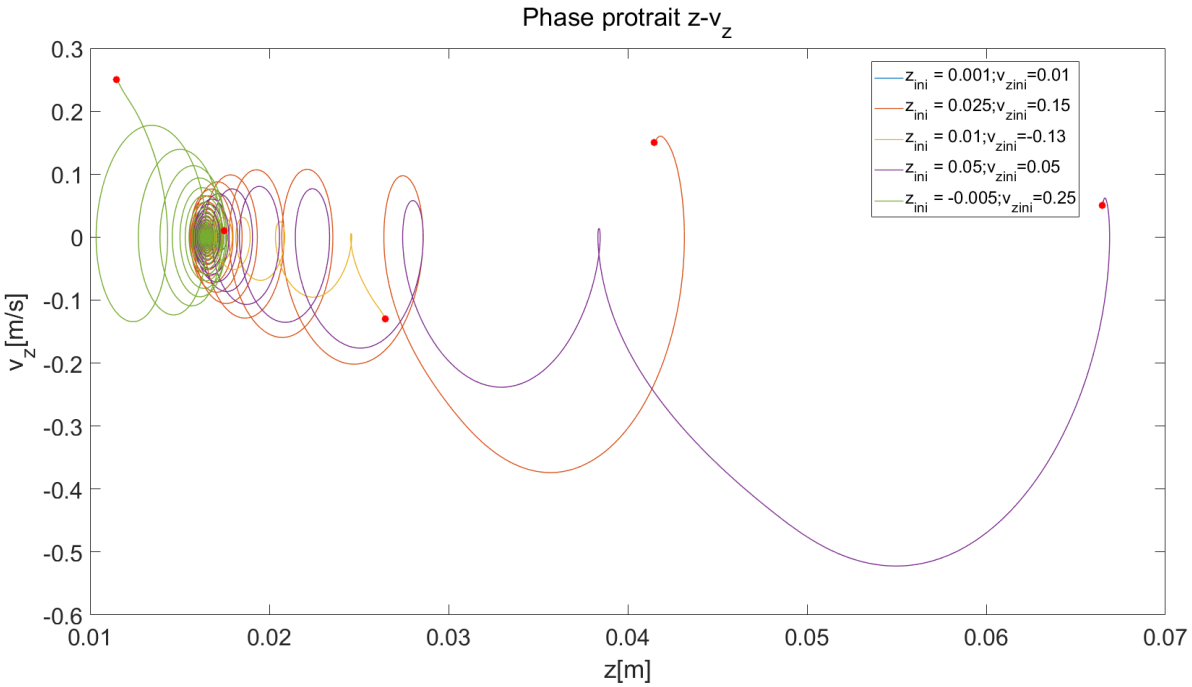


*Figure 4. 14 Phase portrait of the vehicle* $z-\dot{z}$ *for different initial perturbations when* $v=352.9$ **[m/s]**

As can be seen, it shows different trajectory patterns from that of case 1 and the system is stable for all examined perturbations. Hence, the horizontal velocity of vehicle may influence the stable region of initial conditions and this will be discussed in detail in subsequent sections.

### *4.3.2. Representative mechanical system*

Before studying the effects of EMS system on the instability of vehicle with varying velocity, one can first find a representative mechanical system and seek for its behavior under different velocity in order to set a reference for the non-linear system.

Now imagine a system in which the vehicle is moving at constant velocity on the beam and they are connected by a spring and dash-pot (*Figure 4. 15*), where the stiffness of the spring is $k=\frac{Mg}{\delta_0}$, the damping is $c=\zeta\cdot 2\sqrt{kM}$, $\zeta$ is damping ratio. Then one could find the stable region of velocity for fixed mass and damping of this system and the velocity versus mass relationship for different damping.

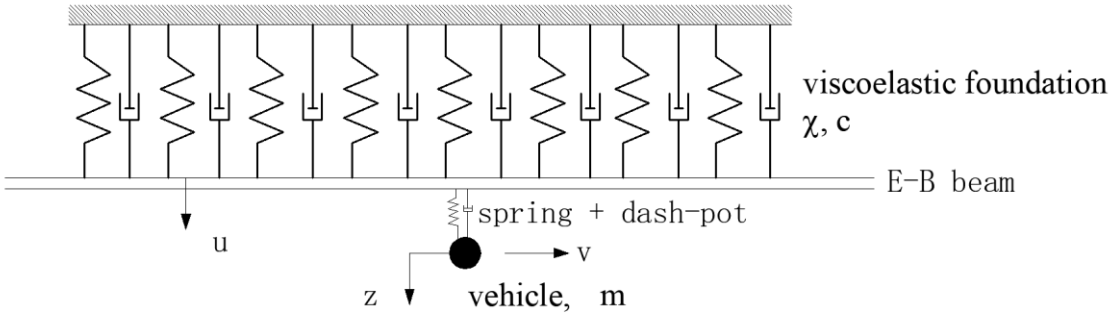


*Figure 4. 15 Representative linear mechanical system*

1. Stable region of velocity for fixed mass and damping

The stability region of the linear mechanical system for three different damping ratios at the velocity range from 0 to $1.5v_{crit}$ is shown below (*Figure 4. 16*)

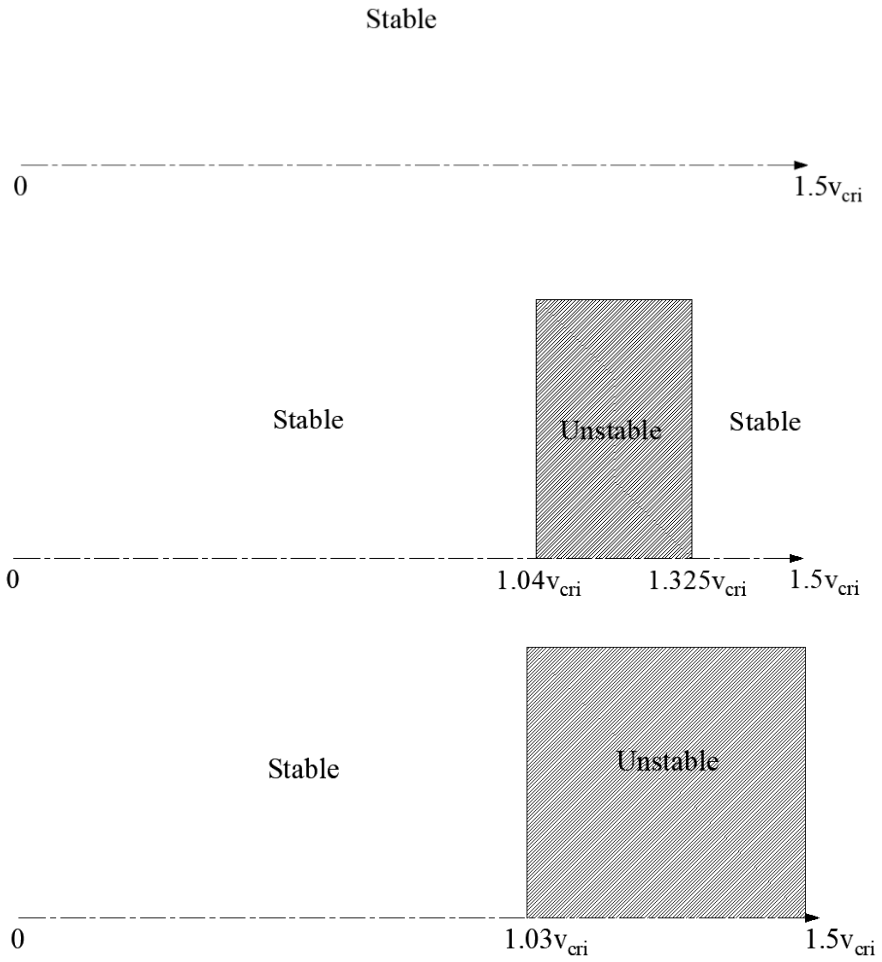


*Figure 4. 16 Stability region of velocity for mechanical system with different damping. The damping ratio is 5%, 0.1%, and 0 from top to bottom*

Where the horizontal axis represents the ratio of actual horizontal velocity and critical velocity, the mass of the vehicle is $m = M$ , the initial perturbations are $z_{ini} = 0.001$ and $v_{zini} = 0$. It is found that the larger the

damping ratio, the narrower the unstable region after the critical velocity. It might because for larger velocity the energy increased by anomalous waves is relatively small and can be damped while for velocity in between the increased energy due to anomalous waves is higher.

2. Velocity versus mass for different damping ratios

As shown in section 2.5.2, the dependency of critical mass (above the value of which the system is unstable) on velocity is important since it can tell us how to keep the system stable. Here the velocity versus mass relationship for this mechanical system is illustrated in *Figure 4. 17*, where the initial perturbations are $z_{ini} = 0.001$ and $v_{zini} = 0$.

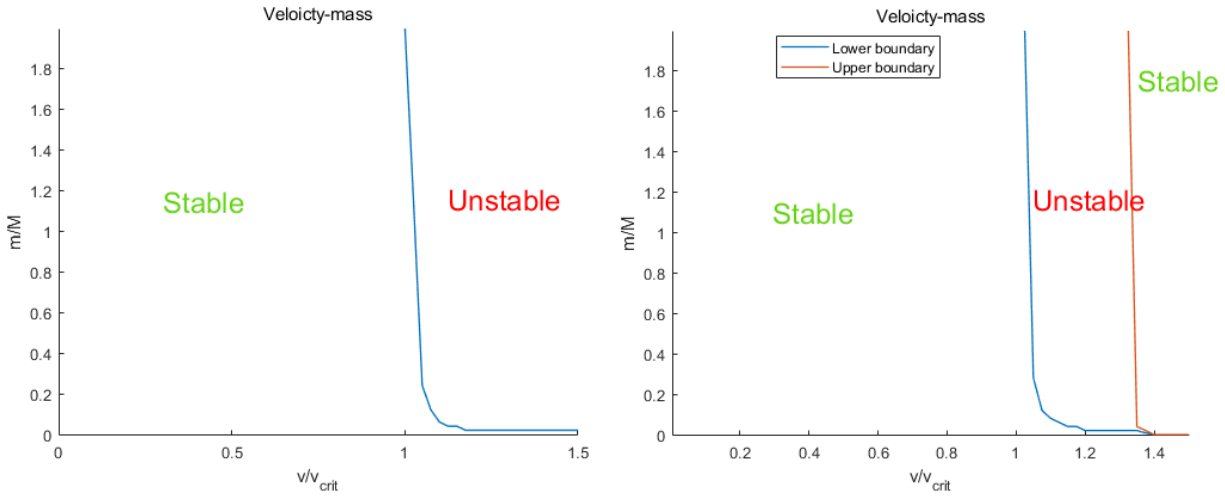


*Figure 4. 17 Velocity versus mass for 0 (left) and 0.1% (right) damping ratio*

It is found that with the increase of damping ratio, the lower boundary will move to the right and the upper boundary will move to the left until they collide with each other and then the whole plane is stable. On the other hand, if the damping ratio decreases, the upper boundary will move to the right and the lower boundary will move to the left until the whole right plane ($v \succ 1.03 v_{crit}$) is unstable.

However, from all above one cannot say for sure the larger the damping ratio, the better to stabilize the system. If one increases the damping ratio to 2 (supercritical damping), the displacements of beam and vehicle for different values of mass would then be like *Figure 4. 18*, where the horizontal velocity is $v = 1.35 v_{crit}$, initial perturbations are $z_{ini} = 0.001$ and $v_{zini} = 0$.

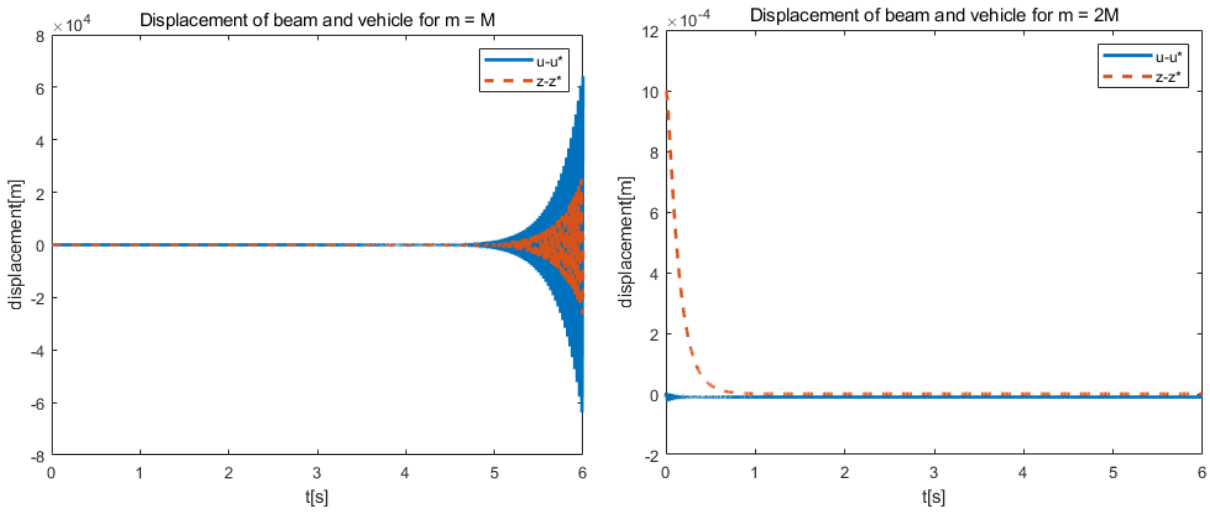


*Figure 4. 18 Displacements of beam and vehicle under supercritical damping ( $\zeta = 2$ ) for m = M (left) and m = 2M (right)*

It is observed that at supercritical velocity the system loses stability when the mass of vehicle is relatively small but returns to stable if the mass increases. This implied that the velocity versus mass relationship would inverse if the damping ratio is too large.

### *4.3.3. Stability versus velocity regions and modes of instability*

Before investigating the relationship of velocity to other parameters of interest, it would be good to firstly obtain the range of velocity at which the system is stable for fixed value of mass, $K_p$ and $K_d$, and then to distinguish the type of instability. This will help us to obtain some useful information to keep on further study. Here, the stability region, as well as the modes of instability, for aforementioned (section 4.3.1) three different combinations of $K_p$ and $K_d$ is computed and shown in *Figure 4. 19* , where the mass of vehicle is $m = M$ , the initial perturbations are $z_{ini} = 0.001$ and $v_{zini} = 0$.

It is found that for the first group (top of *Figure 4. 19*), the system is always stable; for the second group (middle of *Figure 4. 19*), it shows stability when $v \prec 1.075v_{crit}$ , then the system becomes unstable with exponentially increase in response from $1.075v_{crit}$ to $1.2v_{crit}$ , after which a stable limit cycle appears; for the third group (bottom of *Figure 4. 19*), the system is unstable at both lower (from 0 to $0.75v_{crit}$ ) and higher velocity (from $1.075v_{crit}$ to $1.5v_{crit}$ ), what's more, there is only stable limit cycle and no exponential increase in this case.

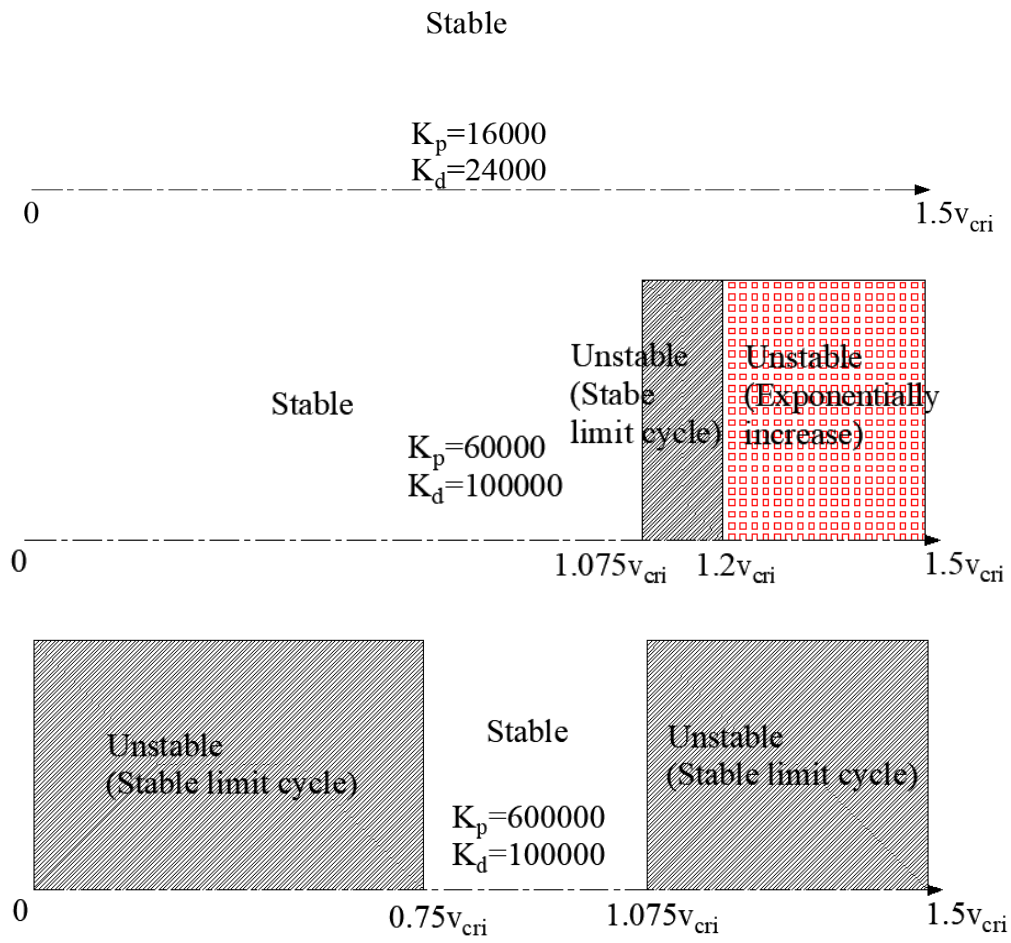


*Figure 4. 19 Stability region of velocity for EMS system with different control gains and modes of instability. The value of* $K_p$ and $K_d$ *are {16000,24000}, {60000,100000}, {600000,100000} from top to bottom*

From above one can obtain the following information: 1. The EMS system can delay the onset of instability at supercritical velocity; 2. The EMS system could be stable even at supercritical velocity if control gains are chosen properly; 3. The EMS system can interact with the guideway which makes the system stable even with inappropriate values of control gains. Instability which occurs at subcritical velocity is due to the unproper set of control gains (here the value of $K_p$ is too large), while the reason for instability at supercritical velocity is the combined effects of EMS and anomalous Doppler waves [28].

The limit cycle mostly results from the on/off switch control of electric current. For instance, take one point from case 3 of *Figure 4. 19* ( $K_p = 600000$ and $K_d = 100000$ ) which is located at $v = 0.5v_{crit}$ . The displacements of beam and vehicle with and without on/off control are illustrated in *Figure 4. 20*, where $m = M$ , $z_{ini} = 0.001$, and $v_{zini} = 0$. It is found that once the on/off switch of current is disabled, the response of the system will increase to infinity. This is reasonable as if the value of current is negative, the control system is trying to repel the vehicle rather than attract. Nevertheless, the force is concerned with the square of current (see eq. 4.2), which means the attraction force is increased instead, and this might lead to the instability as the force behaves opposite to what the control system wants it to.

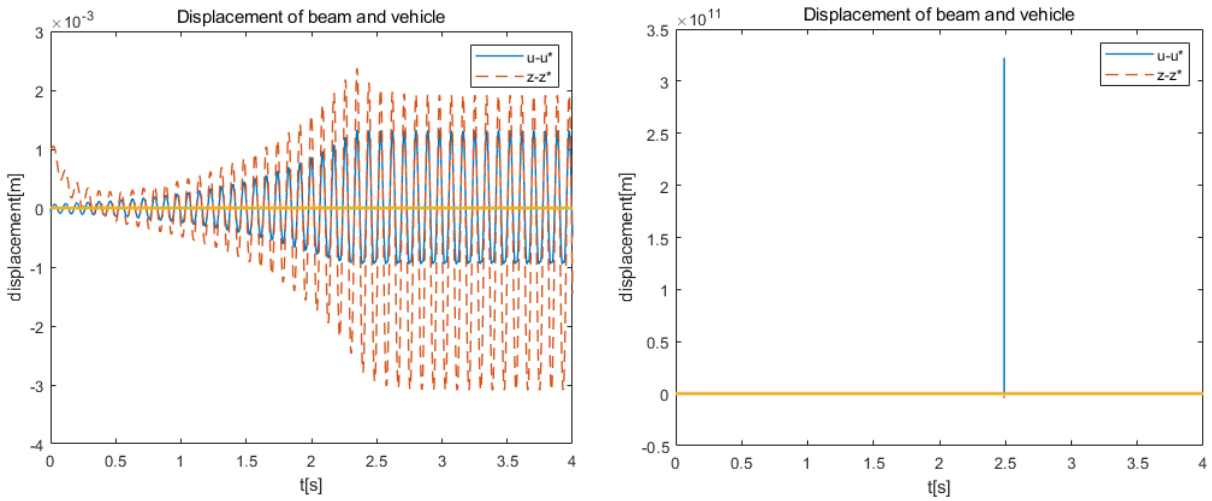


*Figure 4. 20 Displacements of beam and vehicle with (right) and without (left) switch on/off control of current*

However, even there is no on/off control, the system could also step into limit cycle and one example is case 3 of *Figure 4. 19* at $v = 0.75v_{crit}$. The response with and without on/off control is shown in *Figure 4. 21*, where $m = M$, $z_{ini} = 0.01$, and $v_{zini} = 0.05$ (a bit larger initial perturbations are used to decrease the simulation time before the limit cycle is reached).

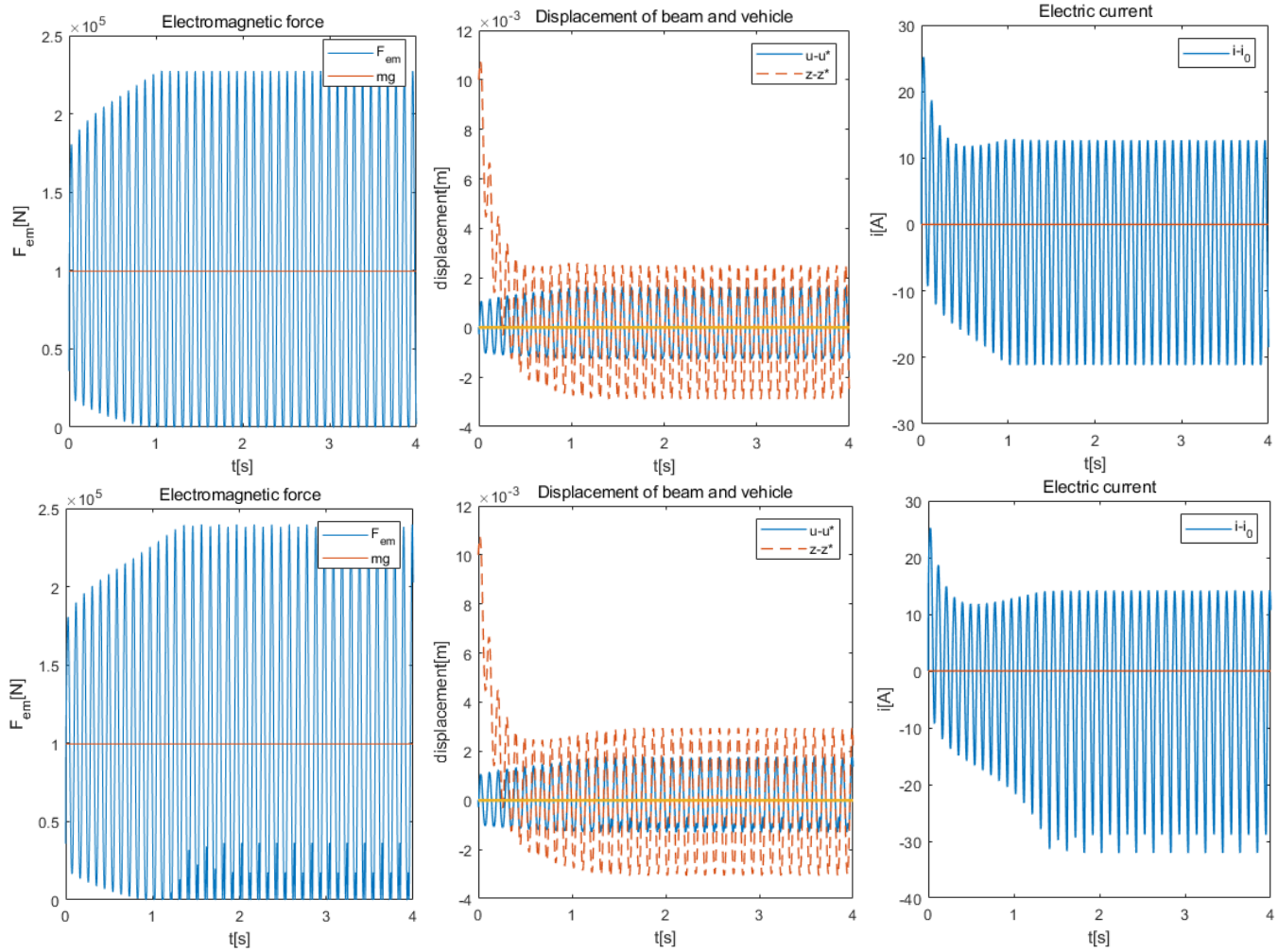


*Figure 4. 21 Response of system with (top) and without (bottom) on/off control*

As can be seen, the limit cycle doesn't vanish but is transformed from standard one to irregular. The reason is that even if the electric current is becoming negative, and subsequently the electromagnetic force becomes larger than 0 and remain attractive. However, the force is still smaller than gravity of vehicle, which means no sudden downward acceleration will happen but only the upward acceleration will decrease, and if this deviation to the original purpose of the control system is acceptable, then the system will keep running like a cycle, but with different amplitudes.

### *4.3.4. Stability-instability perturbation boundary for different load velocities*

For the linear mechanical system, there is only stable or unstable fixed point. If it's attracting, then the system will be stable for the whole phase plane of initial perturbations and no boundary would exist. However, in the non-linear system, there is a region of initial conditions that leads the system settles to the equilibrium point, while outside of this region, the response of the system increases exponentially.

As elaborated in section 4.3.1, the horizontal velocity of vehicle might influence the stability region of initial conditions (it should be noted that the value of control gains also shows great impact [8], which is already investigated and not of interest here). Hence, the stable boundary of initial perturbation versus velocity is illustrated for fixed value of mass, $K_p$ and $K_d$.

The results are shown in *Figure 4. 22*, where $K_p = 16000$, $K_d = 24000$ and $m = M$. It can be told that the stability region grows when the velocity increases from below $v_{crit}$, then reaches maximum when $v = v_{crit}$, after which the stability region decreases to the initial state. What's more, the lower boundary is nearly unchanged when the velocity is varying.

One can conclude that the larger the initial perturbation of displacements, the wider the stability region of initial velocity, and there is no obvious effect of velocity on stability boundary of initial conditions. In addition, the instability phenomenon shown in *Figure 4. 11* is due to the negative initial perturbation on position of vehicle.

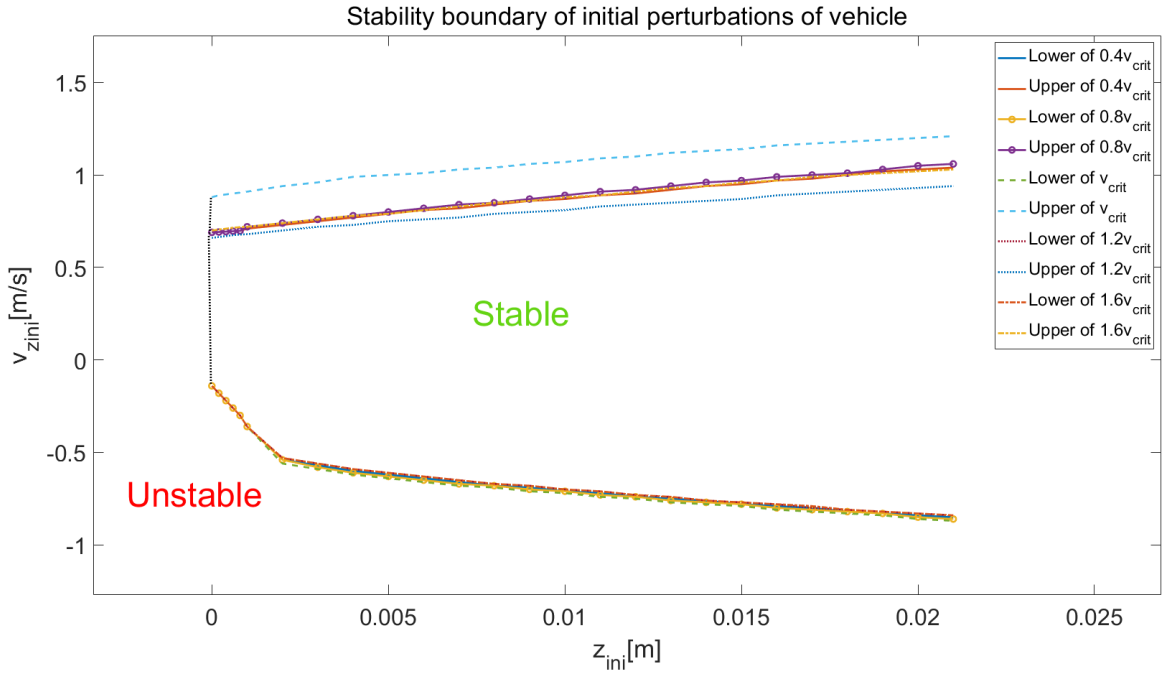


*Figure 4. 22 Stability boundary of initial perturbations for different horizontal vehicle velocity*

### *4.3.5. System stability versus velocity and control gains*

The control gain is important in EMS system and it affects the behavior of the whole system by even a tiny variation. Thus, to better understand the effects of EMS on instability of vehicle-beam coupled system, it's necessary to figure out the dependency of $K_p$ and $K_d$ on velocity. This section focuses on illustrating velocity versus control gains relationship by defining boundary between stability and instability.

To be noted, one should pay attention to the setting of unstable conditions for numerical simulations as there are two modes of instability (exponentially increase and limit cycle). In small time scope (save time running simulations), if the condition is only based on the occurrence of an exponentially increasing instability as "Once the displacement of vehicle is ten times larger than the initial perturbation, the system is unstable", one would miss many other unstable cases and the computed relationship is inaccurate. Here, the author used empirical conditions of instability obtained from large number of simulations and two representative cases are shown below (*Figure 4. 23*)

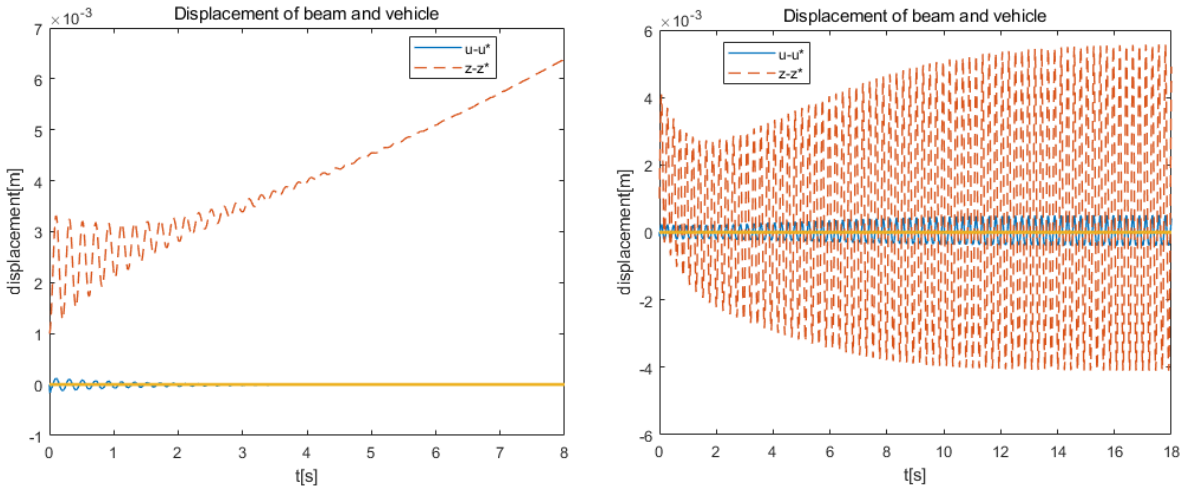


*Figure 4. 23 Representative instability modes except exponentially increase, where* $v = 0.65v_{crit}$, $m = M$, $K_d = 24000$, $K_p = 13000$ *(left) or* $K_p = 22000$ *(right)*

On the left of *Figure 4. 23* the displacement of vehicle is increasing at very small rate and even after 8 seconds, the difference from initial perturbation is not dramatic while on the right, stable limit cycle appears. Both instability patterns cannot be distinguished by the "large displacement" criterion, hence one should conclude at least 3 conditions of instability corresponding to instability with small increasing rate, large increasing rate, and limit cycle.

1. Velocity versus $K_p$

The left of *Figure 4. 24* shows the outcomes for $K_d = 24000$, where $m = M$, $z_{ini} = 0.001$, $v_{zini} = 0$. One can observe that there are two boundary lines, inside of those the system is stable and vice versa. On the one hand, the system can be always stable at the tested velocity range if $K_p$ is located at appropriate range ($13700 \sim 16500$). On the other hand, it's unstable for all velocity if $K_p$ is too large or small ($\{\geq 29500\} \vee \{\leq 13600\}$). Furthermore, two special cases indicated by black dotted line in the left *Figure 4. 24* are found. In case 1, the system is unstable for small velocity, then becomes stable around critical velocity, and

returns to unstable after passing critical velocity. This is in accordance to bottom case of *Figure 4. 19* where $K_p$ is relatively large compared with $K_d$ and the results are confirmed. It's reasonable that the system loses stability at small velocity, even in the non-moving case, as the value of $K_p$ is unproper. As for supercritical velocity, the wave effects would cause instability. The interesting phenomenon happens when it's located at certain range near the critical velocity, where the system will maintain stable. It might because the damping effects of the foundation is increasing with velocity and to some extent, the extra energy of vehicle resulted from large value of $K_p$ is transferred to the foundation. Whereas for case 2, it shows opposite characteristics with case 1 in which the system is stable for most of the velocity range but unstable when it's near but larger than the critical velocity. The stability results from the proper choice of $K_p$ and once after critical velocity, the anomalous wave effects may present greater impact and cause instability. However, what's strange is that the stability happens again at even larger velocity region and it's because of the combined effects of wave and EMS system.

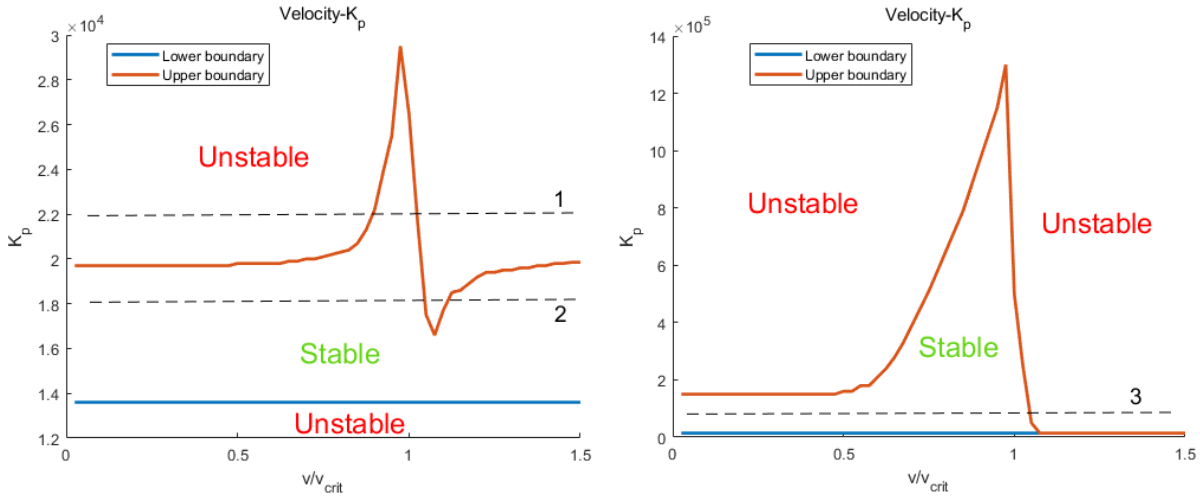


*Figure 4. 24 Velocity versus* $K_p$ *with* $K_d = 24000$ *(left) and* $K_d = 100000$ *(right)*

The right of *Figure 4. 24* shows the results for $K_d = 100000$, where $m = M$, $z_{ini} = 0.001$, $v_{zini} = 0$. It can be told that with the increase of $K_d$ the stable region of $K_p$ before critical velocity will get wider (from 14000 to 150000 in this case) and the maximum permissible value will significantly increase when near the critical velocity (highest at $v = 0.975 v_{crit}$). However, once after the critical velocity, the upper boundary will drop dramatically and hit the lower boundary which leads to the instability of the whole right plane ($v \succ 1.075 v_{crit}$). The special case 3 indicated by black dotted line is in accordance to middle of *Figure 4. 19*, and this confirms that at the supercritical velocity region, the stability of the system is dependent on the interaction of the wave effects and EMS control gains.

Examples of the response of system for above mentioned 3 special cases are illustrated in *Figure 4. 25*.

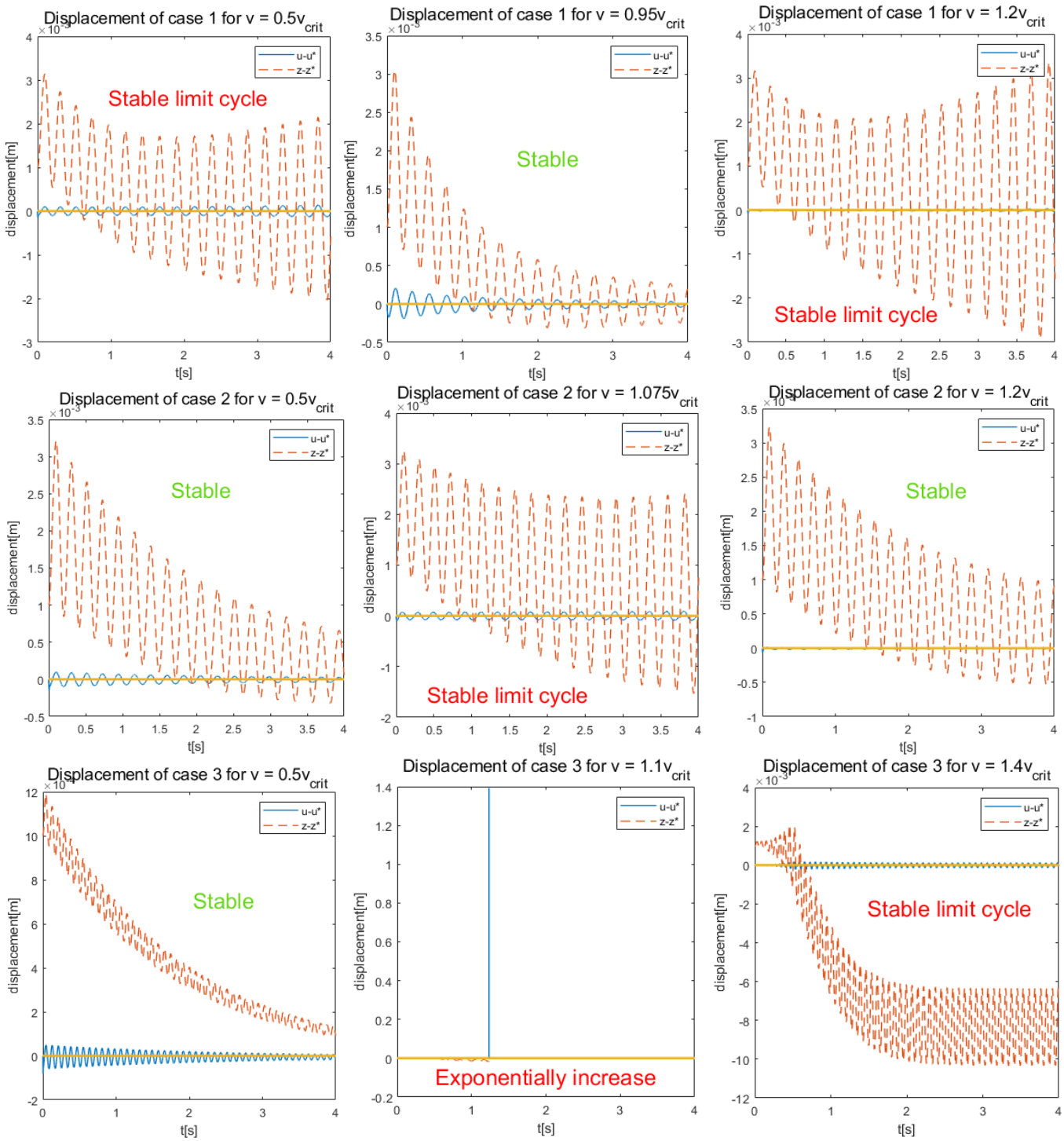


*Figure 4. 25 Representative examples of special case 1 (top), case 2 (middle), case 3 (bottom)*

One can tell that for case 1 and case 2, the unstable mode only consists of limit cycle (if one increases the time scale, it will be clearer), while for case 3 exponential increasement is found. What's more, the existence of Hopf bifurcation in EMS system is also confirmed as for fixed value of velocity and $K_d$ (left of case 1 and 2 in *Figure 4. 25*), the system will be transformed from stable state to limit cycle when $K_p$ increases.

2. Velocity versus $K_d$

The relationship between velocity and $K_d$ with a fixed value of $K_p$ (16000) is illustrated in *Figure 4. 26*, where $m = M$ , $z_{ini} = 0.001, v_{zini} = 0$.

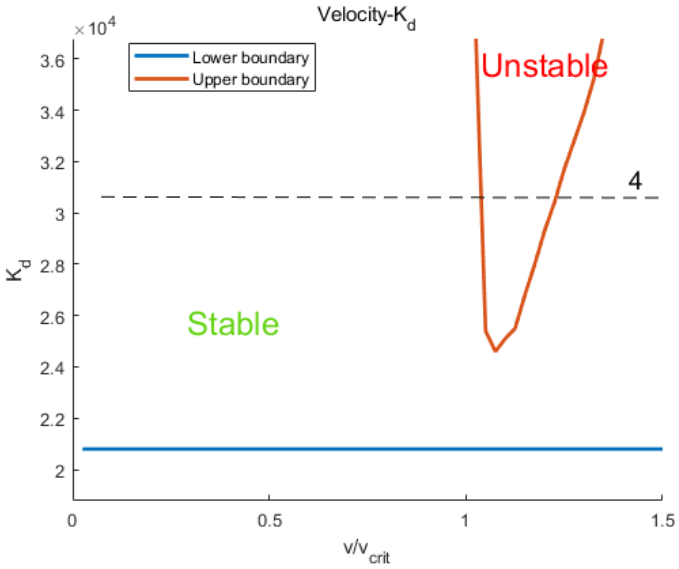


*Figure 4. 26 Velocity versus* $K_d$ *with* $K_p = 16000$

It is found that the system is stable at subcritical velocity for proper range of $K_d$ ($20900 \sim 36000$), once passing the critical velocity, the upper stable boundary (red line of *Figure 4. 26*) of $K_d$ will suddenly drop and gradually rise up with the increase of velocity. The characteristics of the case 4 indicated by black dotted line is somewhat like those of mechanical system (*Figure 4. 16*) as it has three stages: 1. Stability at subcritical velocity; 2. Instability at around critical velocity; 3. Stability at even larger velocity. The difference is that in mechanical system, the instability region of velocity becomes narrower with the increase of damping ratio, here however, it will get wider with the increase of $K_d$. The second stage is caused by wave effects and the third stage is might due to the energy introduced by anomalous waves gets smaller with the increase of velocity and then can be consumed by EMS system. The larger the $K_d$, the smaller the energy can be absorbed by EMS (not sure), the higher the horizontal velocity to stabilize the system.

### *4.3.6. Velocity versus mass of vehicle*

As elaborated in section 2.5.2 and 4.3.2, the mass of vehicle also shows essential effects on the stability and there is an unstable region of mass after critical velocity for the linear mechanical system. Along this line, the relationship between velocity and mass in EMS system is worth to study and it would reveal some nature of this kind of system.

Three different instability conditions are set in the numerical simulations, which are corresponding to stable limit cycle, small increasing rate, and large increasing rate accordingly. The results are shown in *Figure 4. 27*, where $z_{ini} = 0.001, v_{zini} = 0$, $K_p = 16000$, $K_d = 24000$.

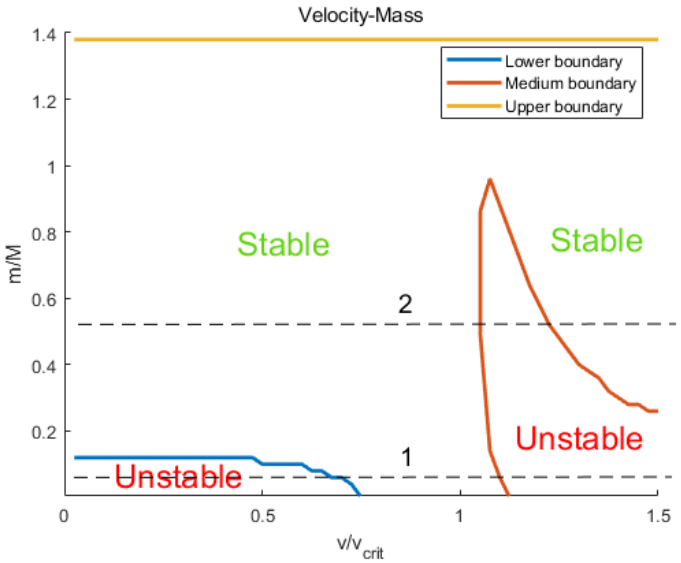


*Figure 4. 27 Velocity versus mass of EMS for* $K_p = 16000$ *and* $K_d = 24000$

It's not hard to tell that at subcritical velocity, the EMS system can lose stability for both small and large mass of vehicle which is quite different from that of mechanical system as latter is stable for any mass at subcritical velocity. This phenomenon also happens at supercritical velocity, and the unstable region of mass (inside of red line in *Figure 4. 27*) is maximum near the critical velocity and decreases as speed goes up. What's more, for supercritical velocity the system will experience instability-stability-instability when the mass is increasing gradually and this is opposite to that of mechanical system where the trend is stability-instability-stability.

Two special cases are found and indicated by black dotted line in *Figure 4. 27*. For case 1, the mass of vehicle is relatively small, and the system is unstable at small velocity, then it becomes stable when speed goes up (still smaller than critical velocity), once after critical velocity, it returns unstable again. This is resulted from the effects of EMS in which the stability range of mass is also dependent on control gains, which means small mass can also cause instability. However, when it's around critical velocity, the damping effects of the foundation will increase through which the energy introduced by EMS can be absorbed and consumed. Once passing critical velocity, the wave effects will interact with EMS and cause instability. Nevertheless, the system can return to stable at even larger velocity as shown by case 2.

To show the trend of variation, response of the system for case 1 are illustrated in *Figure 4. 28* at three different velocities.

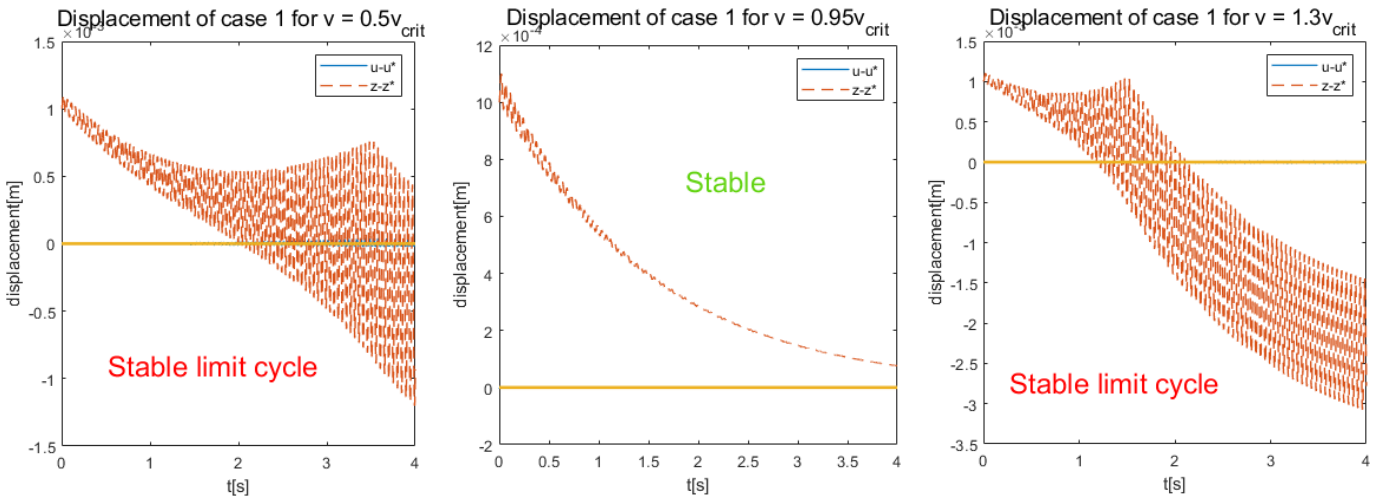


*Figure 4. 28 Representative examples of case 1*

It can be observed that at both instability regions, a stable limit cycle appears (which is not fully shown here) and it's not around the equilibrium point (steady-state position), which is hard to explain as it's caused by the on/off switch control (non-smooth dynamics). In addition, the system will step into stable state from limit cycle when the mass increases and it's like an inverse Hopf bifurcation.

# 5. Analytical Linear Approximations

In the last chapter, the stability of the EMS vehicle-beam coupled system has been studied through time-stepping numerical simulations. To reveal the nature, the non-linear system (eq. 3.1) is linearized here around the steady-state response. The linearized system can allow for eigenvalues analysis such that the onset of instability becomes clearer.

## *5.1.Derivation process of linearization*

Firstly, the system of equations of motion is presented again below

$$\begin{cases} u(t)=\int_0^t g_{EB}(t-\tau)F_{em}(\tau)d\tau+u_f(t) \\ m\ddot{z}(t)=mg-F_{em}(t) \\ F_{em}(t)=\mathrm{sgn}(z(t)-u(t))C\dfrac{i^2(t)}{(z(t)-u(t))^2} \\ \dot{i}(t)=\dfrac{z(t)-u(t)}{2C}[K_p(z(t)-u(t)-\delta_0)+K_d(\dot{z}(t)-\dot{u}(t))+U_0-i(t)R+2C\dfrac{i(t)}{(z(t)-u(t))^2}(\dot{z}(t)-\dot{u}(t))] \end{cases} \tag{5.1}$$

Now one can assume the parameters are composed of two parts which read

$$\begin{cases} u=u_{ss}+u_{tr} \\ z=z_{ss}+z_{tr} \\ F_{em}=F_{emss}+F_{emtr} \\ i=i_{ss}+i_{tr} \end{cases} \tag{5.2}$$

Where $u_{ss}$, $z_{ss}$, $F_{emss}$, and $i_{ss}$ stand for the steady-state response of the system and are known constants (eq. 5.4); $u_{tr}$, $z_{tr}$, $F_{emtr}$, and $i_{tr}$ are the disturbance applied to the equilibrium point (here steady-state). Substituting eq. 5.2 into eq. 5.1, one obtains

$$\begin{cases} u_{ss}+u_{tr}=\int_0^t g_{EB}(t-\tau)F_{emss}d\tau+u_f(t)+\int_0^t g_{EB}(t-\tau)F_{emtr}d\tau \\ \ddot{z}_{tr}=g-\dfrac{F_{emss}+F_{emtr}}{m} \\ F_{emss}+F_{emtr}=C\dfrac{(i_{ss}+i_{tr})^2}{(z_{ss}+z_{tr}-u_{ss}-u_{tr})^2} \\ \dot{i}_{tr}=\dfrac{z_{ss}+z_{tr}-u_{ss}-u_{tr}}{2C}[Kp(z_{ss}+z_{tr}-u_{ss}-u_{tr}-\delta_0)+Kd(\dot{z}_{tr}-\dot{u}_{tr}) \\ \qquad +U_0-(i_{ss}+i_{tr})R+2C\dfrac{i_{ss}+i_{tr}}{(z_{ss}+z_{tr}-u_{ss}-u_{tr})^2}(\dot{z}_{tr}-\dot{u}_{tr})] \end{cases} \tag{5.3}$$

Eq. 5.3 can be further simplified as the correlation between different steady-state parameters are known and they read

$$\begin{aligned} u_{ss} &= \int_0^t g_{EB}(t-\tau)F_{emss}d\tau + u_f(t) \\ z_{ss} - u_{ss} &= \delta_0 \\ F_{emss} &= mg \\ i_{ss} &= \sqrt{\frac{F_{emss}\delta_0^2}{C}} \\ U_0 &= i_{ss}R \end{aligned} \tag{5.4}$$

Where the steady-state vibration of beam $u_{ss}$ is equal to the superposition of force-vibration under constant force $F_{emss}$ and free-vibration $u_f$ with steady-state as initial conditions. Then one can rewrite eq. 5.3 as follows

$$\begin{cases} u_{tr} = \int_0^t g_{EB}(t-\tau)F_{emtr}d\tau = f_1 \\ z_{tr} = \int_0^t g_{mtr}(t-\tau)F_{emtr}d\tau + z_{ftr} = f_2 \\ F_{emtr} = C\dfrac{(i_{ss}+i_{tr})^2}{(\delta_0 + z_{tr} - u_{tr})^2} - mg = f_3 \\ \dot{i}_{tr} = \dfrac{\delta_0 + z_{tr} - u_{tr}}{2C}[Kp(z_{tr}-u_{tr}) + Kd(\dot{z}_{tr}-\dot{u}_{tr}) - i_{tr}R + 2C\dfrac{i_{ss}+i_{tr}}{(\delta_0 + z_{tr} - u_{tr})^2}(\dot{z}_{tr}-\dot{u}_{tr})] = f_4 \end{cases} \tag{5.5}$$

Where $f_1$, $f_2$, $f_3$, and $f_4$ are used to denote the right-hand side of equations in eq. 5.5, $z_{tr}$ is written in form of convolution integral and $z_{ftr} = z_{tr}(0) + v_{zini}t$ represents the free-vibration part of perturbation of vehicle from the equilibrium point, $g_{EB}$ is already computed by numerical simulations (section 4.1.1), $g_{mtr}(t) = -\frac{t}{m}$. Since the velocity of beam and vehicle ($\dot{u}_{tr}$ and $\dot{z}_{tr}$) appear in eq. 5.5, it's necessary to derive both by using Leibniz integral rule ($\frac{d}{dx}\left(\int_{a(x)}^{b(x)} f(x,t)dt\right) = f(x,b(x))\cdot\frac{d}{dx}b(x) - f(x,a(x))\cdot\frac{d}{dx}a(x) + \int_{a(x)}^{b(x)}\frac{\partial}{\partial x}f(x,t)dt$) and they read

$$\begin{cases} \dot{u}_{tr}(t) = \int_0^t \dot{g}_{EB}(t-\tau)F_{emtr}d\tau + g_{EB}(0)F_{emtr} \\ \dot{z}_{tr}(t) = \int_0^t \dot{g}_m(t-\tau)F_{emtr}d\tau + v_{zini} \end{cases} \tag{5.6}$$

Where $g_{EB}(0)$ is Green's function of beam evaluated at $t=0$, which is supposed to be 0 analytically, and yet a tiny non-zero value obtain from numerical computation is taking into account. Then one can apply Taylor expansion to $f_3$ and $f_4$ around the following points

$$\begin{cases} u_{tr}=0 \\ \dot{u}_{tr}=0 \\ z_{tr}=0 \\ \dot{z}_{tr}=0 \\ i_{tr}=0 \end{cases} \tag{5.7}$$

By which $f_3$ and $f_4$ are linearized and the results are shown below

$$\begin{cases} F_{emtr}=k_{f1}u_{tr}+k_{f2}z_{tr}+k_{f3}i_{tr} \\ \dot{i}_{tr}=k_{i1}u_{tr}+k_{i2}\dot{u}_{tr}+k_{i3}z_{tr}+k_{i4}\dot{z}_{tr}+k_{i5}i_{tr} \end{cases} \tag{5.8}$$

Where $k_{f1}=\frac{2Ci_{ss}^2}{\delta_0^3}$ , $k_{f2}=-\frac{2Ci_{ss}^2}{\delta_0^3}$ , $k_{f3}=\frac{2Ci_{ss}}{\delta_0^2}$ , $k_{i1}=-\frac{\delta_0 K_p}{2C}$ , $k_{i2}=\frac{\delta_0(-K_d-\frac{2Ci_{ss}}{\delta_0^2})}{2C}$ , $k_{i3}=\frac{\delta_0 K_p}{2C}$ , $k_{i4}=\frac{\delta_0(K_d+\frac{2Ci_{ss}}{\delta_0^2})}{2C}$, $k_{i5}=-\frac{\delta_0 R}{2C}$.

After substituting eq. 5.8 into eq. 5.5, one can solve the linearized system by applying Laplace transform to eq. 5.5 and the system in Laplace domain are presented as following

$$\begin{cases} u_{tr}(s)=g_{EB}(s)\cdot(k_{f1}i_{tr}(s)+k_{f2}u_{tr}(s)+k_{f3}z_{tr}(s)) \\ z_{tr}(s)=g_m(s)\cdot(k_{f1}i_{tr}(s)+k_{f2}u_{tr}(s)+k_{f3}z_{tr}(s)) \\ si_{tr}(s)=k_{i1}u_{tr}(s)+sk_{i2}u_{tr}(s)+k_{i3}z_{tr}(s)-z_{tr}(0)+sk_{i4}z_{tr}(s)+k_{i5}i_{tr}(s) \end{cases} \tag{5.9}$$

Where the initial perturbations are all zero except the displacement of vehicle $z_{tr}(0)$. Eq. 5.9 is linear algebraic and can be solved analytically, they read

$$\begin{cases} u_{tr}(s)=\dfrac{g_{EB}k_{f1}z_{tr}(0)}{g_{EB}k_{f1}k_{i2}s+g_m k_{f1}k_{i4}s+g_{EB}k_{f1}k_{i1}-g_{EB}k_{f2}k_{i5}+g_{EB}k_{f2}s+g_m k_{f1}k_{i3}-g_m k_{f3}k_{i5}+g_m k_{f3}s+k_{i5}-s} \\ z_{tr}(s)=\dfrac{g_m k_{f1}z_{tr}(0)}{g_{EB}k_{f1}k_{i2}s+g_m k_{f1}k_{i4}s+g_{EB}k_{f1}k_{i1}-g_{EB}k_{f2}k_{i5}+g_{EB}k_{f2}s+g_m k_{f1}k_{i3}-g_m k_{f3}k_{i5}+g_m k_{f3}s+k_{i5}-s} \\ i_{tr}(s)=-\dfrac{z_{tr}(0)\cdot(g_{EB}k_{f2}+g_m k_{f3}-1)}{g_{EB}k_{f1}k_{i2}s+g_m k_{f1}k_{i4}s+g_{EB}k_{f1}k_{i1}-g_{EB}k_{f2}k_{i5}+g_{EB}k_{f2}s+g_m k_{f1}k_{i3}-g_m k_{f3}k_{i5}+g_m k_{f3}s+k_{i5}-s} \end{cases} \tag{5.10}$$

One can tell from eq. 5.10 that the stability of the system (real part of roots of denominator) is indeed concerned with the four parameters discussed in the last chapter, which are velocity ( $g_{EB}$ and $g_m$ ), control gains ( $K_p$ and $K_d$ ), and mass of vehicle respectively.

## 5.2.Validation of linearized system

To verify the linearized system, one can generate the response of this system by the same numerical method (ODE45) and compare the outcomes with that of non-linear system. The comparison is illustrated in *Figure 5. 1* under different velocity.

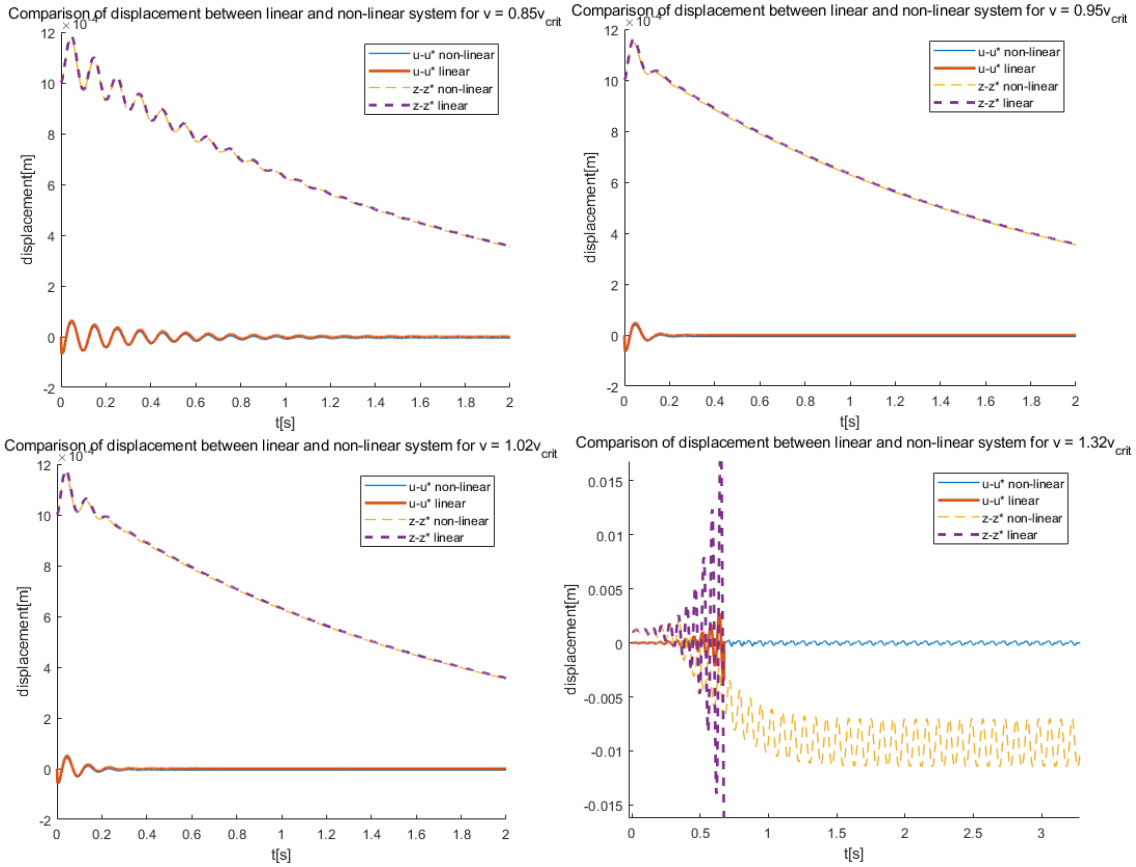


*Figure 5. 1 The comparison of displacement of beam and vehicle between linear and non-linear system at different horizontal velocity. Black and rea solid line represent the displacement of beam in non-linear and linear system, yellow and purple dash line represent the displacement of vehicle in non-linear and linear system. Where* $K_p = 60000$, $K_d = 100000$, $m = M$ , $z_{ini} = z_{trini} = 0.001$, *and* $v_{zini} = 0$.

It is found that the behavior of the linearized system is nearly the same as the one of non-linear system when the velocity is located at stable region. While the velocity goes up, as shown in bottom right of *Figure 5. 1*, the non-linear system is unstable and reaches limit cycle, the linearized system, on the other hand, shows exponentially increase which is to be expected since the limit cycle is a characteristic of non-linear systems. One can conclude that the linearization of the system is successful and correct.

As explained before (section 2.1.1), the prerequisite of the linearization and is that the perturbation around the fix point must be small enough (to guarantee of accuracy of the results). Thus, examples are illustrated in fig. to show the effects of large initial perturbations.

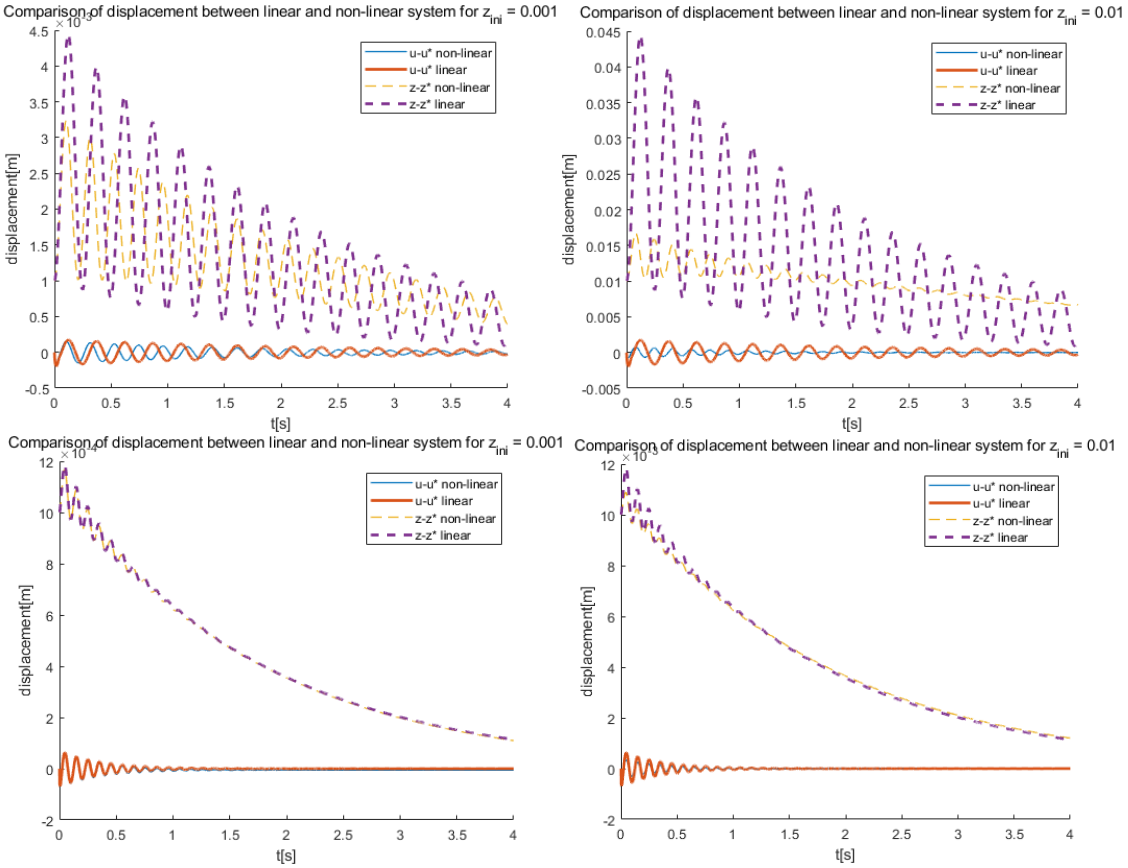


*Figure 5. 2 Effects of relatviely large initial perturbation on accuracy of linearization for 2 groups of control gains. Top:* $K_p = 16000$, $K_d = 24000$*; Bottom:* $K_p = 60000$, $K_d = 100000$

It is observed that for group 1 (top of *Figure 5. 2*) of control gains, the error of linearization is around 35% and 180% (calculated through displacement of vehicle) with $z_{ini} = 0.001$ and $z_{ini} = 0.01$ respectively. While for group 2 (bottom of *Figure 5. 2*), the error of linearization is around 1% and 10% with $z_{ini} = 0.001$ and $z_{ini} = 0.01$ respectively. One can conclude that the safe region of initial perturbation in which the linearized system has high accuracy of prediction is dependent on the value of $K_p$ and $K_d$. The larger the $K_p$ and $K_d$, the more accurate under large disturbance. This is reasonable as the neglected quadratic terms in the process of Taylor expansion is a function of $K_p$ and $K_d$.

# 6. Conclusion and Recommendations

This chapter summarizes all the results of this thesis and relates them to the original problem statement and research objectives. In the last, some recommendations for future study on this topic is proposed.

## *6.1.Conclusions*

There are three main goals in this thesis: 1. Find a numerical method to solve the non-linear one-dimensional system; 2. Investigate the dynamic behavior of the EMS vehicle-beam coupled system using the improved model, and illustrate the effects of the EMS system on vehicle instability at different horizontal velocity by comparing with EMS system in simplified model. 3. Linearize the system around the steady-state position.

The Green's function of beam in the moving reference frame at different velocity is determined numerically using two methods (convolution integral from Fourier domain or superposition of wave modes in Laplace domain), and it is validated by comparing the steady-state solution under moving constant force with that obtained analytically. To take the initial conditions into account, free-vibration part of beam is also determined numerically and it is corroborated by comparing the initial shape of beam with the analytical one where the error is around 6%. By linear assumptions of convolution integral in tiny time interval, a time-stepping scheme in MATLAB using function of ODE45 is designed and it is validated by a limit case study where the mass of vehicle is quite small.

A representative linear mechanical system in which the beam and vehicle are connected by spring and dash-pot is designed. For fixed value of mass, it is found that the system is always stable at subcritical velocity with all tested damping values, while at supercritical velocity, the larger the damping ratio, the narrower the unstable region after the critical velocity, and the system can be always stable at tested range of velocity ($0 \sim 1.5v_{crit}$) for a relatively large damping. For different damping ratios, the stable domain of mass at different velocities is illustrated and it is found that at subcritical velocity, the system is always stable while at supercritical velocity, there exists an instability region of mass and the system can only be stable for small value of mass. The larger the damping ratio, the narrower of this instability region and if the damping is zero, then the whole right mass-velocity plane ($v \succ 1.03v_{crit}$) is unstable. However, for overcritical damping (e.g., damping ratio is 2), it is observed that at supercritical velocity the system loses stability when the mass of vehicle is relatively small but returns to stable if the mass increases.

The value of control gains in EMS system is determined based on the simplified two degrees of freedom system, where the effects of velocity are neglected. The stable range of velocity with fixed value of mass in one-dimensional EMS vehicle-beam coupled system is investigated for three different groups of control gains (two stable and one unstable in simplified system) and it is found that

1. For the cases of control gains which can stabilize the simplified system, the one-dimensional guideway has no negative effect on the stability of the vehicle at subcritical velocity. Whereas at supercritical velocity, the EMS system can counteract the wave-induced instability and stabilize the vehicle if the control gains are chosen properly.

2. For the case of control gains which are chosen incorrectly such that the simplified system is unstable, the one-dimensional guideway has positive effects which can stabilize the vehicle at certain range

around critical velocity and this is counter-intuitive as the system is transformed from unstable to stable with the increase of speed.

Besides, the system stability versus velocity and proportional control gains for fixed value of $K_d$ and mass is determined to explain such a stability transition at both subcritical and supercritical velocity. It is found that the stable domain of $K_p$ will become wider with the increase of velocity and reaches maximum when it's near the critical velocity, and once after the critical velocity the upper stability boundary will suddenly drop and decreases the stable domain of $K_p$ dramatically. This situation is more significant with large value of $K_d$ in which the upper boundary will collide with the lower boundary and leads to the instability for all values of $K_p$ at supercritical velocity. Here, three special cases are found and case 1 is in accordance to the aforementioned stability transition phenomenon. The second special case confirms that the EMS system can counteract the wave-induced instability and transform the system from unstable to stable at supercritical velocity.

Moreover, the stable domain of mass at different velocities in EMS system for fixed value of control gains has been analyzed. It is found that for the appropriate value of control gains determined from simplified two degrees of freedom EMS system, there exists a range of mass under which the system is always stable. Two special cases are observed and they confirm the positive effects of one-dimensional beam and the counteractive effects of EMS system on anomalous Doppler waves at supercritical velocity.

## *6.2.Recommendations*

Two special phenomena are observed in this thesis:

1. The positive effects of one-dimensional guideway at subcritical velocity which can stabilize the system with unproper value of control gains.

2. The counteractive effects of EMS system on wave-induced instability at supercritical velocity which can stabilize the system with proper choice of control gains.

The mechanisms for the two observations have not been thoroughly investigated in this thesis. Thus, it would be highly recommended to investigate the physical nature of these two cases for future studies.

As the system is linearized successfully in this thesis, it would be instructive to analyze the eigenvalues of the linearized system to offer a more complete picture of the system's instability

For quantitative improvement, one can also consider the shear effects of the beam by introducing Timoshenko beam theory and take the periodicity of the supports into account.

# 7. REFERENCES


[1] A. Schafer and D. G. Victor, "The future of mobility of the world population," Transportation Research Part A - Policy and Practice, vol. 34, p. 171, 2000.

[2] H. Ritchie, "Our World in Data - Climate change and flying> what share of global CO2 emissions come from aviation?," University of Oxford, 22nd October 2020. [Online]. Available: https://ourworldindata.org/co2-emissions-from-aviation. [Accessed 13th April 2022].

[3] "The SciFi Story Robert H. Goddard Published 100 Years Ago". Available: gizmodo.com.

[4] Musk, Elon (12 August 2013). "Hyperloop Alpha" . Retrieved 13 August 2013.

[5] Opgenoord, Max M. J. "How does the aerodynamic design implement in hyperloop concept?". Mechanical Engineering. MIT - Massachusetts Institute of Technology. Retrieved 16 September 2019.

[6] "China testing super-maglev train that runs at 1,000 km/h". People's Daily Online. 11 March 2018. Retrieved 26 August 2021.

[7] S. Earnshaw, "On the nature of molecular forces which regulate the constitution of the Luminiferous Ether.," in *Transcription of the Cambridge Philosophical Society*, Cambridge, M. A. of St. John's Colledge, 1842, p. 97.

[8] J. Mas Soldevilla, "Dynamic analysis and stability study of the electromagnetic suspension levitation system of the Hyperloop, "

[9] S. H. Strogatz, Nonlinear Dynamics and Chaos with Applications to Physiscs, Biology, Chemistry and Engineering, Boulder, CO: Westview Press, 2015.

[10] A. M. G. Jacob and N. M. V. Monteiro, "A new concept of superelevation in magnetic levitation - prodynamic," *Transportation Systems and Technology*, vol. 4, no. 4, pp. 77-111, 2018.

[11] "Maglev Trains - McGill," 2007. [Online]. Available:
https://www.cs.mcgill.ca/~rwest/wikispeedia/wpcd/wp/m/Maglev_train.htm. [Accessed 28th February 2022].

[12] J. D. Yau, "Vibration Control of Maglev vehicles travelling over a flexible guideway," *Journal of Sound and Vibration*, vol. 321, pp. 184-200, 2009.

[13] Z. Liu, Z. L. Li and X. Li, Maglev Trains: Key Underlying Technologies, Berlin: Springer, 2015.

[14] "Technology Development - Hardt Hyperloop," 2020. [Online]. Available: https://hardt.global/technology-development/. [Accessed 2nd March 2022].

[15] "Magnetic Levitation - UCSB Physics," [Online]. Available:
https://web.physics.ucsb.edu/~lecturedemonstrations/Composer/Pages/68.78.html. [Accessed 2nd March 2022].

[16] X. Chen, W. Ma and S. Luo, "Study on stability and bifurcation of electromagnet-track beam coupling system for EMS maglev vehicle," *Nonlinear Dynamics*, vol. 101, pp. 2181-2193, 2020.

[17] X. Chen, W. Ma, S. Luo and R. Zou, "A vehicle-track beam matching index on EMS Maglev transportation system," *Arch. Appl. Mech.*, 2019.

[18] H. S. Han, B. H. Yim, N. J. Leec, Y. C. Hur and S. S. Kim, "Effect of the guideway's vibrational characteristics on the dynamics of a Maglev vehicle," *Vehicle System Dynamics*, vol. 47, no. 3, pp. 309-324, 2009.

[19] J. Hu, W. Ma, X. Chen and S. Luo, "Levitation Stability and Hopf Bifurcation of EMS Maglev Trains," *Mathematical Problems in Engineering*, 2020.

[20] J. H. Li, J. Li and D. F. Zhou, "Self-excited vibration problems of Maglev vehicle-bridge interaction system," *J. Cent. South Univ.*, vol. 21, no. 11, pp. 4184-4192, 2014.

[21] X. Li, D. Wang, D. Liu, L. Xin and X. Zhang, "Dynamic analysis of the interactions between a low-to-medium speed Maglev train and a bridge: field test results of two typical bridges," *Proceedings of the Institution of Mechanical Engineers, Part F: Journal of Rail and Rapid Transit*, vol. 36, pp. 2039-2059, 2018.

[22] X. H. Shi, L. H. She and W. S. Chang, "The bifurcation analysis of the EMS maglev vehicle-coupled-guideway system," *Acta Mechanica Sinica*, vol. 36, pp. 634-640, 2004.

[23] H.-S. Han and D.-S. Kim, Magnetic Levitation: Maglev Technology and Applications, Dordrecht: Springer, 2016.

[24] P. Wolf and e. al., "P, I, D, PI, PD, and PID Control," University of Michigan, December 2021.

[25] O.-o. c. system, "X-Engineer," [Online]. Available: https://x-engineer.org/on-off-control-system/. [Accessed 7th April 2022].

[26] A. Urquizo. [Online]. Available: https://en.wikipedia.org/wiki/PID_controller#/media/File:PID_en.svg. [Accessed 7th April 2022].

[27] A.R.M Wolfert, “WAVE EFFECTS IN ONE-DIMENSIONAL ELASTIC SYSTEMS INTERACTING WITH MOVING LOADS” *1999*.

[28] A. V. Metrikine, H. A. Dieterman (1996), “INSTABILITY OF VIBRATIONS OF A MASS MOVING UNIFORMLY ALONG AN AXIALLY COMPRESSED BEAM ON A VISCOELASTIC FOUNDATION” Journal of Sound and Vibration (1997) 201(5), 567-576.

[29] A. B. Faragau, T. Mazilu, A. V. Metrikine, T. Lu, K. N. van Dalen, "Transition radiation in an infinite one-dimensional structure interacting with a moving oscillator-the Green’s function method," *Journal of Sound and Vibration*, vol. 492, 2021.